Iranian Journal of Fuzzy Systems
Volume 23, Number 5, (2026), pp. 37-66
Original paper

Hybrid fuzzy-MPC approach for secure consensus in time-delayed multi-robot networks under sensor and actuator attacks

P. Yu [1], W. Ul Hassan [2], A. Mishal [3], A. Smerat [4], A. U. Khan Niazi [5] and N. Iqbal [6]

[1] *Hefei Technology College, Hefei, 230012, Anhui, PR China*
[2,3] *Department of Mathematics, Faculty of Sciences, University of Mianwali, 42200, Mianwali, Punjab, Pakistan*
[4] *Hourani Center for Applied Scientific Research, Al-Ahliyya Amman University, Amman 19328, Jordan*
[4] *Department of Biosciences, Saveetha School of Engineering, Saveetha Institute of Medical and Technical Sciences, Chennai, 602105, India*
[5] *Department of Mathematics and Statistics, The University of Lahore, Sargodha 40100, Pakistan*
[6] *Department of Mathematics, College of Science, University of Ha'il, Ha'il 2440, Saudi Arabia*

yuping@htc.edu.cn, waqarulhassan439@gmail.com, abeehamishal96@gmail.com, smerat.2020@gmail.com
azmatullah.khan@math.uol.edu.pk, naveediqbal1989@yahoo.com

Abstract

This paper addresses the consensus problem in multi-robot systems subject to time delays, unknown nonlinearities, and cyber-physical attacks. To effectively handle uncertainties and mitigate the adverse effects of malicious disruptions, a Type-3 fuzzy logic system is introduced to construct a robust hybrid control framework. The considered network is exposed to sensor attacks, actuator attacks, and Byzantine disruptions, where particular emphasis is placed on mitigating sensor and actuator attacks. The proposed controller is designed to achieve two main objectives: minimizing the consensus error among robots and maintaining balanced update behavior during communication processes. Furthermore, a constrained control strategy based on Model Predictive Control (MPC) is incorporated to optimize resource utilization and enhance system security. By embedding security constraints into the MPC formulation, the proposed approach effectively reduces the influence of sensor attacks on the networked robots. To validate the effectiveness of the developed framework, the Duffing-Holmes chaotic system is employed as a benchmark model, demonstrating improved performance under communication delays and cyber-physical disturbances. In addition, Lyapunov-Krasovskii functional analysis combined with Linear Matrix Inequalities (LMIs) is utilized to establish the convergence and stability conditions of the multi-robot network. Finally, extensive simulation results are provided to verify the theoretical findings and demonstrate the robustness and effectiveness of the proposed strategy under attack scenarios and time-delay conditions.

Keywords: Multi-robot systems, consensus control, cyber-physical attacks, Type-3 fuzzy logic, model predictive control (MPC), time-delay systems, byzantine fault tolerance, duffing-Holmes chaotic system.

1 Introduction

Multi-robot networks have emerged as a promising paradigm for intelligent and autonomous systems, enabling cooperative decision-making, distributed coordination, and efficient execution of complex tasks. However, communication delays, unknown nonlinearities, physical constraints, and cyber-physical attacks can significantly degrade networked robotic performance, creating a strong need for secure and resilient control strategies. Recent advances in intelligent modeling and adaptive robotic technologies have improved the capability of robotic systems to handle uncertainty and achieve flexible operation, but the effects of communication constraints and malicious attacks on distributed consensus

Corresponding Author: A. U. Khan Niazi
Received: November 2025; Revised: May 2026; Accepted: July 2026.
https://doi.org/10.22111/ijfs.2026.53689.9505

remain largely unexplored [4, 42]. Multi-agent exploration and physically adaptive millirobots have demonstrated effective coordination and manipulation capabilities, yet their frameworks do not address secure networked consensus under delays and adversarial disturbances [16, 53]. Delay-aware coordinated tracking using event-triggered communication and MPC has improved control efficiency and resource utilization, but the simultaneous presence of unknown nonlinearities and multiple cyber-physical attacks has not been considered [31]. Event-triggered security control, advanced robotic mechanisms, and robust neural-network-based tracking have enhanced resilience against DoS attacks, physical uncertainties, and disturbances; however, their application to delayed multi-robot consensus under combined attack scenarios remains limited [5, 18, 21]. Robust constraint-following and adaptive dynamic programming have further strengthened control performance for uncertain robotic and nonlinear systems, but distributed consensus with communication delays and simultaneous sensor, actuator, and Byzantine attacks remains insufficiently investigated [11, 28].
Intelligent robotic systems increasingly rely on optimization, learning, and adaptive control to improve autonomy, flexibility, and reliability. Real-time motion planning and multimodal intelligence have enhanced robotic adaptability and decision-making, but their application to delayed multi-robot consensus under cyber-physical attacks remains limited [34, 59]. Adversarial learning methods have also strengthened privacy protection against malicious manipulation, yet they do not address resilient coordination and consensus in networked robotic systems [6]. Neural-network-based computation and transformer-based reinforcement learning have shown potential for robotic control and intelligent decision-making; however, communication delays, unknown nonlinearities, and multiple attack mechanisms are not jointly considered [20, 52]. Event-triggered adaptive control and unsupervised monitoring can improve communication efficiency and system supervision, but their applicability to secure multi-robot consensus remains limited [37], [40]. Fuzzy fault-tolerant control, adaptive safety control, and reinforcement learning have improved robustness against delays, faults, uncertainties, and emergency conditions; nevertheless, simultaneous sensor, actuator, and Byzantine attacks in networked robots remain insufficiently addressed [9, 19, 45]. Predictive fault diagnosis and sample-efficient reinforcement learning have improved system monitoring and learning efficiency, but they do not directly resolve secure distributed consensus under delayed and adversarial communication [2, 25]. Multi-sensor fusion has enhanced sensing and intelligent assistance in robotic applications, although secure coordination under malicious disturbances is not considered [55]. Cooperative reinforcement learning, adaptive fuzzy control, and event-triggered fuzzy consensus have strengthened intelligent decision-making and uncertain multi-agent regulation, but a unified treatment of communication delays and multiple cyber-physical attacks is still lacking [27, 36, 49]. Resilient adaptive dynamic programming and autonomous robotic path planning have improved networked control and navigation performance, yet combined sensor, actuator, and Byzantine attacks within delayed multi-robot consensus remain unexplored [48, 58]. Robust H2/H∞ and data-driven sliding-mode methods provide effective disturbance rejection and uncertainty compensation, but they do not simultaneously address unknown nonlinearities, communication delays, and multiple attack types in multi-robot consensus [14, 47]. Privacy-preserving consensus and cooperative robotic systems have improved information security and coordination, but they do not simultaneously address communication delays, unknown nonlinearities, and cyber-physical attacks in multi-robot networks [22, 26]. Fuzzy adaptive force control has enhanced robotic performance under uncertain environments, while neural adaptive control and intelligent obstacle detection have strengthened robustness and perception; however, their application to secure distributed consensus remains limited [30, 33, 50]. Learning-based imaging, semantic grasping, and programmable soft-robotic structures have advanced information processing, manipulation, and physical adaptability, but network-level security and cooperative consensus are not considered [3, 23, 51]. Constraint-based servo control and safe human-robot motion planning have improved tracking and operational safety, yet cyber attacks and resilient multi-robot coordination remain outside their scope [8, 39]. Complex dynamic modeling and safety-critical reinforcement learning have addressed uncertain dynamics and obstacle avoidance, but delayed and attack-resilient multi-robot consensus has not been investigated [32, 46]. Magnetically actuated millirobots have demonstrated flexible multimodal manipulation, although networked coordination and attack resilience remain unexplored [15]. Path planning and sensor calibration have improved autonomous navigation and measurement reliability, but do not address combined uncertainty and cyber-physical threats in cooperative robotic systems [54, 60]. Neural-network-based sliding-mode control and information-propagation models have strengthened robustness and system analysis, yet distributed consensus under delays and malicious disturbances remains unaddressed [35, 44].
Fractional-order fuzzy synchronization with time-varying delays, advanced legged-robot control, and wireless power-transfer technologies have enhanced nonlinear regulation, mobility, and autonomous operation, but they do not provide an integrated solution for secure multi-robot consensus [13, 38, 43]. Anonymous formation control and faulty-substructure detection have contributed to secure coordination and network fault identification, although simultaneous sensor, actuator, and Byzantine attacks remain insufficiently considered [12, 24]. Structural optimization and behavioral modeling have improved engineering-system performance, but their application to delayed and attack-resilient multi-robot consensus is limited [29, 41]. Cooperative positioning has strengthened distributed localization for underwater robots, yet unknown nonlinearities and adversarial disturbances are not addressed [7]. Predictive control and variable-

morphology soft robotics have improved maneuverability and adaptability, but secure networked consensus remains unexplored [1, 10]. Robust constraint-following, fuzzy uncertainty compensation, and robotic posture optimization have enhanced nonlinear control and physical performance, but communication delays and multiple cyber-physical attacks are not jointly considered [17, 56, 57]. Overall, existing studies largely address individual aspects of uncertainty, communication, physical robustness, or security. In contrast, the proposed framework jointly considers time delays, unknown nonlinearities, sensor attacks, actuator attacks, and Byzantine disruption through an integrated Type-3 fuzzy logic and security-constrained MPC strategy, aiming to enhance consensus accuracy, attack resilience, stability, and control-resource utilization.

The resulting control policies ensure a seamless trade-off between coordination efficiency and system feasibility under real-world constraints. An innovative event-triggered strategy based on adaptive switching thresholds is devised, allowing control updates only when necessary, thus significantly reducing communication overhead. Under decentralized communication settings, a finite-time distributed observer is formulated to estimate the leader's motion state accurately. To handle uncertainties and external perturbations, fuzzy logic systems are employed to capture unmodeled nonlinearities, and disturbance observers are designed to compensate for both environmental disturbances and internal estimation errors. The developed approach guarantees that all closed-loop signals remain bounded while effectively suppressing elastic deformations, ensuring the coordinated and reliable behavior of flexible multi-robot systems even in dynamic and uncertain environments.

Motivated by the above discussion, we wind up following the main contributions in this paper,

1. A hybrid control architecture is developed that combines a Type-3 fuzzy logic system with a predictive control structure. This design specifically addresses the challenges posed by unknown nonlinearities, time delays, and targeted sensor and actuator attacks within multi-robot systems.

2. The proposed control strategy incorporates real-time security constraints into a Model Predictive Control (MPC) formulation. This allows the system to minimize consensus errors while actively mitigating the influence of sensor falsification and actuator interference, ensuring reliable decision-making under adversarial conditions.

3. Theoretical guarantees of system stability and consensus are established using Lyapunov-Krasovskii functional methods and Linear Matrix Inequality (LMI) analysis. To demonstrate the controller's effectiveness, simulations based on the Duffing-Holmes chaotic system are presented, validating performance in the presence of cyber-physical disturbances and communication delays.

4. A major strength of the proposed hybrid control architecture lies in the effective integration of Type-3 fuzzy logic with model predictive control. The Type-3 fuzzy logic system can accurately approximate unknown nonlinear behaviors and represent higher-level uncertainties, while the MPC component computes optimal control inputs subject to system constraints and reduces the influence of sensor and actuator attacks. Together, these two methods provide stronger robustness, higher consensus precision, and more secure and stable operation even in the presence of time delays and adversarial disturbances, offering better performance than using fuzzy control or MPC alone.

1. Section 1, presents a detailed discussion on Type-3 Fuzzy robots, we also present the previous research contribution for the stability of robotic control systems.

2. Section 2 presents the preliminary definitions, communication strategy using graph theory, formation of the problem, approximation error, and consensus error for robots.

3. Section 3, presents the effect of sensor attack and actuator attack on robots under the necessary conditions.

4. In Section 4, we developed the Type-3 Fuzzy logic controller, which is a robot controller under all uncertainties.

5. Section 5, provided the model predictive controller for the estimated control signals, calculated all results, and we proved the model,s stability by using Lyapunov functional and Linear matrix inequality.

6. In Section 6, we present the numerical simulations to prove the above theoretical results and set up MATLAB simulations.

7. In Section 7, we make conclusions for this paper.

2 Preliminary actions and definitions of problems

2.1 Graph theory according to multi-robotics

To model the relationship between individual robots within a system, graph theory is used: $\mathcal{G} = (\nu, \varepsilon)$ where nodes (ν) represent each robot and edges (ε) represent the pathway or connection between them, where $\nu = \{$ 0,1,2,... $\}$ are nodes set. Where $\varepsilon \subseteq \nu \times \nu$ is a set of edges. where (l,m) $\in \nu \times \nu$ (robot-l can obtain data from robot-m) and ϕ= $[\varphi_{lm}] \in \mathbb{R}^{w\times w}$ the adjacency matrix and it is define as φ_{ll}= 0 and φ_{lm} ¿ 0 if (l,m) $\in \varepsilon$ and $\varphi_{lm} = 0$ otherwise.

2.2 Problem formulation

The l-th robot has given dynamics which are shown in Figure (1). This can be written as

$$a_l(u+1) = h_l(a_l(u-T)) + k_l(a_l(u-T))v_l(u) \ l = 1...w. \tag{1}$$

Where unknown functions $h_l(a_l(u-T))$ and $k_l(a_l(u-T))$ are estimated by the network with hint of Type-3 FLSs as $\widehat{h}_l(a_l, \mu_{hl})$ and $\widehat{k}_l(a_l, \mu_{kl})$, where μ_{hl} and μ_{kl} are tunable parameters of $\widehat{h}_l(a_l, \mu_{hl})$ and $\widehat{k}_l(a_l, \mu_{kl})$, respectively. The Eq.(1) becomes:

$$\widehat{a}_l(u+1) = \widehat{h}_l(a_l, \mu_{hl}) + \widehat{k}_l(a_l, \mu_{kl})v_l(u), \ l = 1...w. \tag{2}$$

Where $v_l(u)$ is the control signal that can be changed to $v_l(u) = v_{1l}(u) + v_{2l}(u).v_{1l}(u)$. Can be formulated as

$$v_{1l}(u) = \widehat{k}_l^{-1}(a_l(u), \mu_{kl}(u))[-\widehat{h}_l(a_l(u), \mu_{hl}(u)) + \alpha_l a_l(u)]. \tag{3}$$

Where α_l is a matrix written as

$$\alpha_l = \begin{bmatrix} 0 & 1 & \cdots & 0 \\ \vdots & \vdots & \ddots & \vdots \\ 0 & 0 & ... & 1 \\ -\eta_{l,1} & -\eta_{l,2} & \cdots & -\eta_{l,p} \end{bmatrix}. \tag{4}$$

Where $\eta_l, m, m = 1, ..., p$ are constant and p is the number of robots, according to the Hurwitz stability criterion, is fulfilled. As a result, the behavior of the $l-th$ robot is shown.

$$\begin{aligned} a_l(u+1) = \alpha_l a_l(u) + \gamma_l v_{2l}(u) + \big[h_l(a_l(u-T)) - \widehat{h}_l(a_l(u), \mu_{hl}(u)) + k_l(a_l(u-T)) - \widehat{k}_l(a_l(u), \mu_{kl}(u))v_l(u)\big], \\ \text{where } l = 1, 2 \ldots w. \end{aligned} \tag{5}$$

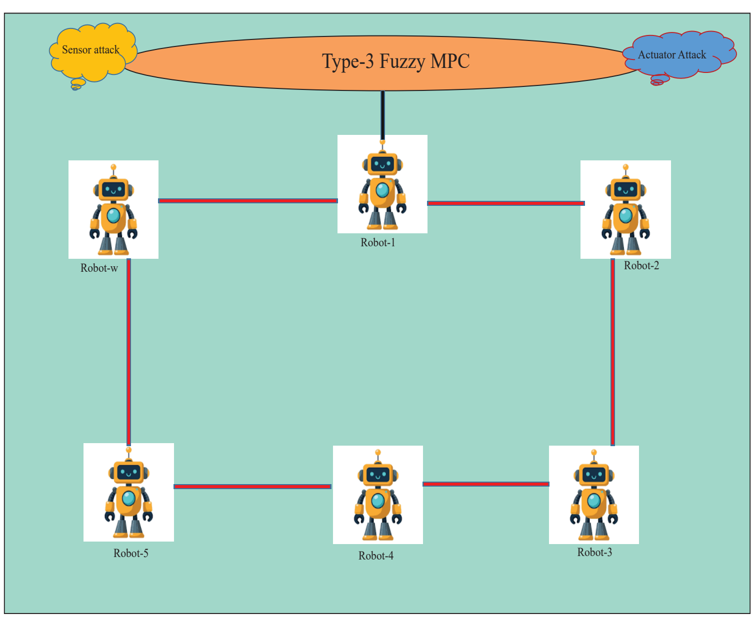

Figure 1: Structure of robots with Type-3 Fuzzy MPC Controller.

2.2.1 Approximation error

By using the approximation error as

$$\beta_l(u) = [h_l(a_l(u-T)) - \widehat{f}_l(a_l(u), \mu_{hl}(u)) + k_l(a_l(u-T)) - \widehat{k}_l(a_l(u), \mu_{kl}(u)v_l(u)]. \tag{6}$$

It takes the form of

$$a_l(u+1) = \alpha_l a_l(u) + \beta_l(u) + \gamma_l v_{2l}(u), \quad l = 1...w. \tag{7}$$

Where $\gamma_l = [0, ..., 1]^\tau$. Then, AE can be written as

$$\beta_l(u) = \alpha_{el} a_l(u-e). \tag{8}$$

Where e is an unknown but bounded constant delay, and $\alpha_{el} \in \mathbb{R}^{n\times n}$ is a known constant matrix representing the approximation error dynamics with compatible dimensions Eq. (4)
By substituting Eqs. (7) and (8), we obtain:

$$a_l(u+1) = \alpha_l a_l(u) + \alpha_{el} a_l(u-e) + \gamma_l v_{2l}(u), \quad l = 1...w. \tag{9}$$

2.2.2 Consensus error

The consensus error is defined as:

$$d_l(u) = a_l(u) - \frac{1}{w}\sum_{m=1}^{w} \vartheta_{lm} a_m(u), \qquad l = 1...w. \tag{10}$$

We consider Eq. (9) and Eq. (10), and we obtain:

$$d_l(u+1) = a_l(u+1) - \frac{1}{w}\sum_{m=1}^{w} \vartheta_{lm} a_l(u+1), \quad l = 1...w.$$

$$= \alpha_l a_l(u) + \alpha_{el} a_l(u-e) + \gamma_l v_{2l}(u) - \frac{1}{w}\sum_{m=1}^{w} \vartheta_{lm}(\alpha_m a_m(u) + \alpha_{em} a_m(u-e) + \gamma_m v_{2m(u)}). \tag{11}$$

Where coefficient ϑ_{lm} are taken from adjacency matrix ϕ.

3 Sensor and actuator attacks

In cyber-physical robotic systems, sensor and actuator components interact closely with the underlying physical processes, making them vulnerable to malicious interventions. When such systems are subjected to adversarial conditions, particularly in multi-robot or networked robotic frameworks, it becomes essential to ensure stability and robustness against potential attacks.
To characterize these threats, the sensor attack is represented as:

$$\delta_{\widehat{s}}(u, a_l(u)), \tag{12}$$

while the actuator attack is modeled as:

$$\delta_{\widehat{a}}(u, a_l(u)). \tag{13}$$

To more accurately capture realistic cyber-physical attack scenarios, the sensor attack is formulated as a combination of false data injection (i.e., corrupted measurements) and denial-of-service (i.e., intermittent data loss). In contrast, the actuator attack is modeled as adversarial perturbations directly affecting the control inputs. All attack signals are assumed to be bounded, ensuring analytical tractability.
If $\delta_{\widehat{s}}(u, a_l(u))$ and $\delta_{\widehat{a}}(u, a_l(u))$ are nonzero then the dynamics of $l-th$ robotics is expressed as. If a sensor attack is added to the multi-robot $l-th$ dynamics, then Eq. (1) can be rewritten as:

$$a_l(u+1) = h_l(a_l(u-T)) + k_l(a_l(u-T))v_l(u) + \delta_{\widehat{s}}(u, a_l(u+1)\ u \geq 0 \ and\ l = 1...w. \tag{14}$$

Where $\delta_{\widehat{s}}(u, a_l(u+1))$ is a sensor attack on multi robotics where $a_l(u+1)$ represent the dynamics of $l-th$ robots
If $\delta_{\widehat{s}}(.,.) \neq 0$ then the sensor attack can be seen in the dynamics $l-th$ of the robots, or if $\delta_{\widehat{s}}(.,.) = 0$ then the dynamic

system $l-yh$ remains unchanged.
Also, if
The control signal $v_1(u)$ also gets changed by the attack, so it can be described as.

$$\tilde{v}_l(u) = v_l(u) + \delta_{\widehat{a}}(u, a_l(u)) \ u \geq 0 \ l = 1...w. \tag{15}$$

Where $v_l(u)$ is control signal and $\tilde{v}_l(u)$ is control signal with actuator attack and $\delta_{\widehat{a}}(.,.)$ is actuator attack capture on control signal. If $\delta_{\widehat{a}}(.,.) \neq 0$, then the multi-robotic control signal gets the actuator attack and it has to be stabilized, while if $\delta_{\widehat{a}}(.,.) = 0$, then $\tilde{v}_l(u) = v_l(u)$
The control signal for the multi-robot system is designed as

$$v_l(u) = v_{1l}(u) + v_{2l}(u).v_{1l}(u).$$

Which was written as Eq. If $\delta_{\widehat{a}}(.,.) \neq 0$, then Eq. (3) becomes.

$$\tilde{v}_{1l}(u) = \widehat{k}_l^{-1}(a_l(u), \mu_{kl}(u))[-\widehat{h}_l(a_l(u), \mu_{hl}(u) + \alpha_l a_l(u)] + \delta_{\widehat{a}}(u, a_l(u)) \ u \geq 0, \quad l = 1...w. \tag{16}$$

Where α_l is explained in matrix Eq. (4) due to which the Hurwitz stability criterion is satisfied.
If $\delta_{\widehat{s}}(u, a_l(u))$ and $\delta_{\widehat{a}}(u, a_l(u))$ are zero, then the $l-th$ dynamics of multi-robotic will continue as.

4 Type-3 fuzzy logic systems (FLS).

The Type-3 Fuzzy Logic System describes the uncertainty of the model using bounded membership functions with $\underline{r}_t$ and $\bar{r}_t$ as parameters, in addition to the interval output rules $[\bar{\zeta}_f, \underline{\zeta}_f]$. All these elements contribute to the overall uncertainty set of the system.

- To improve clarity, all variables used in this section are defined here.
- The input variable $a_l(u)$ represents the system state of the l-th robot, where $l = 1, 2, \ldots, p$.
- Each input is associated with fuzzy sets characterized by:
  - center J_l^m
  - width Δ_l^m
- The parameters $\bar{r}_t$ and $\underline{r}_t$ denote the upper and lower uncertainty levels of the membership functions, respectively.
- Each fuzzy rule is indexed by $f = 1, 2, \ldots, N$, and its output is defined by an interval with lower and upper parameters $\underline{\zeta}_f$ and $\overline{\zeta}_f$.
- The rule activation is determined using membership values, resulting in upper and lower firing strengths.
- The final output is obtained by combining all rules using a weighted average.
- The parameters are updated online using the approximation error, where λ represents the learning rate.

The uncertainty modeling in the proposed Type-3 Fuzzy Logic System can be explained as follows
In the proposed Type-3 fuzzy logic system, uncertainty is modeled at multiple levels to better reflect real-world conditions. First, uncertainty in the inputs is represented using upper and lower membership functions, which provide a range of possible values instead of a single precise value. The parameters $\underline{r}_t$ and $\bar{r}_t$ control the spread of these functions and determine the level of uncertainty considered. In addition, each fuzzy rule produces an output in the form of an interval rather than a fixed value, capturing possible variations in system behavior. During rule evaluation, both upper and lower firing strengths are computed, which further represent uncertainty in the rule activation process. Finally, all rules are combined using a weighted average, ensuring that uncertainty is incorporated into the final output. This multi-level approach enables the system to handle nonlinearities and disturbances more effectively. A Type-3 Fuzzy Logic System is developed to approximate the unknown nonlinear dynamics of multi-robot systems suffering from uncertainties and cyber-physical perturbations. To be able to explain the Type-3 Fuzzy Logic System in a comprehensible way, lower-order fuzzy systems are first reviewed. Subsequently, the Type-3 Fuzzy Logic System is illustrated as an extension to the lower-order fuzzy systems.

4.1 Type-1 fuzzy logic system (T1-FLS)

The first type (Type-1) is the simplest kind of fuzzy inference system. Every input variable has a value that is precisely associated with a specific membership function ranging from 0 to 1. The value of membership functions for every input is well-known and does not acknowledge any uncertainty in it. The inference engine is a set of rules that connect the inputs and outputs. Although the Type-1 Fuzzy Logic System is easy to implement and calculate, the information regarding the system is perfectly known to it. That is why it does not work well with noisy systems or with modeling errors or some kinds of disturbing external factors.

4.2 Type-2 fuzzy logic system (T2-FLS)

Type-2 fuzzy logic systems try to overcome these limitations of Type-1 by including uncertainty directly within the membership functions. An input is associated not with a single value, but with a range of possible membership values, known as the footprint of uncertainty. This footprint helps to manage fluctuations in an environment and the effects of noisy data more effectively. The inference stage also works with the upper and lower bounds of the membership, making it more robust. However, the limitation is that Type-2 still assumes that the form of uncertainty is fixed and cannot model any more complex or layered uncertainty.

4.3 Type-3 fuzzy logic system (T3-FLS)

The Type-3 fuzzy logic system (T3-FLS) expands on this notion by adding a further level of uncertainty. This is because in a Type-3 Fuzzy Logic System, uncertainty doesn't just occur within membership functions, but is modeled over many levels. The result is that instead of having one footprint of uncertainty, the system comprises multiple levels of uncertainty that account for the various ways in which the system can be assumed to behave, as determined by adjustable parameters, which will, in turn, vary how narrow or wide uncertainty regions are.
Type-2 fuzzy logic systems (FLS) model uncertainty by incorporating fuzzy membership functions, whereas Type-3 Fuzzy Logic System further extends this capability by capturing multi-level uncertainty not only in the membership functions but also in the rule consequent. As a result, Type-3 Fuzzy Logic System can provide more effective handling of complex nonlinearities, uncertainties, and external disturbances.

4.4 Rule base and inference mechanism

Type-3 Fuzzy Logic System has a similar rule-based approach to a lower-order Fuzzy Logic System that links input to output. The difference is that each rule is calculated over different levels of uncertainty, resulting in multiple responses to a given input. These responses are weighted according to their relative uncertainties, both lower and upper bounds, to capture as many variations as possible and allow the system to approximate more accurately.

4.5 Output representation

The final output of the Type-3 Fuzzy Logic System is obtained by aggregating the contributions of all rules across all uncertainty levels. This aggregation reflects both the variability in the input data and the uncertainty in the system model. By considering multiple uncertainty layers simultaneously, the Type-3 Fuzzy Logic System can produce smoother and more reliable outputs, especially in highly nonlinear and uncertain environments.

4.6 Advantages of Type-3 fuzzy logic system in multi-robot systems

The Type-3 Fuzzy Logic System is used in this work due to it's advantage in handling unknown nonlinear dynamics, time-delay systems, sensor and actuator uncertainties, and cyber-physical attacks. Type-3 Fuzzy Logic Systems have more comprehensive representation for uncertainty compared to type-1 and type-2 fuzzy systems, resulting in the enhancement of approximation accuracy and robustness. So, it can be utilized to design secure consensus control in a multi-robot system under an attack scenario.
Compared with Type-2 fuzzy systems, the proposed Type-3 fuzzy system captures uncertainty in both the membership functions and rule consequent by generating interval-valued outputs. This leads to a tighter bound on the approximation error. As a result, when integrated into the Lyapunov–Krasovskii framework, the derived stability conditions are less conservative, offering enhanced robustness against time delays and cyber-physical attacks.
In recent developments, fractional fuzzy inference systems (FFIS) have been introduced to further improve the modeling capability of fuzzy systems by incorporating fractional-order dynamics. Compared to conventional Type-2 and Type-3

fuzzy systems, fractional fuzzy inference systems can offer enhanced flexibility and memory properties, which are useful for capturing complex temporal dependencies. However, in this work, the Type-3 fuzzy logic system is adopted due to its favorable balance between modeling accuracy and computational tractability, as well as its straightforward integration with the proposed MPC-based control framework. The extension to fractional fuzzy inference systems-based control systems is considered an interesting direction for future research.
Fractional fuzzy inference systems (FFIS) extend the inference mechanism by incorporating fractional-order concepts, which can improve the modeling of complex system dynamics and uncertainties. While Fractional fuzzy inference systems may offer performance benefits in certain scenarios, this work adopts a Type-3 fuzzy system because of its stronger capability to represent multi-level uncertainties and its more suitable integration with the proposed MPC framework.
The Type-3 Fuzzy Logic System (T3-FLS) is employed to effectively capture uncertainties in both the membership functions and the rule consequents. Although higher-order fuzzy systems generally involve increased computational complexity, a compact rule base along with simplified computational procedures is adopted to mitigate this issue. As a result, the proposed controller achieves enhanced robustness against time delays and adversarial attacks without significantly increasing the overall computational burden. Furthermore, the T3-FLS is utilized to approximate unknown system dynamics. In this work, the conventional T3-FLS framework is further improved through the introduction of a novel learning law. In addition, for the online modeling of each robot, two T3-FLS structures are employed to ensure accurate and adaptive system representation.
this is explained as follows.

1. The inputs that are being used are a_l $l = 1...p$.

2. If the $m-th$ fuzzy set for a_l is considered as $\tilde{\mu}_l^m$. Then the associateship for $\tilde{\mu}_l^m$ at the levels of $\underline{r}_t$ and $\overline{r}_t$ are written as:
For upper associateship.

$$\overline{N}_{\tilde{\mu}^m_{l|\overline{r}_t}} = \begin{cases} 1 - \left(\frac{|a_l - J_{\tilde{\mu}_l^m}|}{\underline{\Delta}_{\tilde{\mu}_l^m}}\right)^{\overline{r}_t} \text{ if } J_{\tilde{\mu}_l^m} - \underline{\Delta}_{\tilde{\mu}_l^m} < a_l \leq J_{\tilde{\mu}_l^m} \\ 1 - \left(\frac{|a_l - J_{\tilde{\mu}_l^m}|}{\overline{\Delta}_{\tilde{\mu}_l^m}}\right)^{\overline{r}_t} \text{ if } J_{\tilde{\mu}_l^m} < a_l \leq J_{\tilde{\mu}_l^m} + \overline{\Delta}_{\tilde{\mu}_l^m} \\ 0 \text{ if } a_l > J_{\tilde{\mu}_l^m} + \overline{\Delta}_{\tilde{\mu}_l^m} \text{ or } a_l \leq J_{\tilde{\mu}_l^m} - \underline{\Delta}_{\tilde{\mu}_l^m} \end{cases} \tag{17}$$

$$\overline{N}_{\tilde{\mu}^m_{l|\underline{r}_t}} = \begin{cases} 1 - \left(\frac{|a_l - J_{\tilde{\mu}_l^m}|}{\underline{\Delta}_{\tilde{\mu}_l^m}}\right)^{\underline{r}_t} \text{ if } J_{\tilde{\mu}_l^m} - \underline{\Delta}\tilde{\mu}_l^m < a_l \leq J_{\tilde{\mu}_l^m} \\ 1 - \left(\frac{|a_l - J_{\tilde{\mu}_l^m}|}{\overline{\Delta}_{\tilde{\mu}_l^m}}\right)^{\underline{r}_t} \text{ if } J_{\tilde{\mu}_l^m} < a_l \leq J_{\tilde{\mu}_l^m} + \overline{\Delta}_{\tilde{\mu}_l^m} \\ 0 \text{ if } a_l > J_{\tilde{\mu}_l^m} + \overline{\Delta}_{\tilde{\mu}_l^m} \text{ or } a_l \leq J_{\tilde{\mu}_l^m} - \underline{\Delta}_{\tilde{\mu}_l^m} \end{cases} \tag{18}$$

To avoid ambiguity, activation refers to the firing strength of each fuzzy rule, determined by the input variables and membership functions, whereas the rule expression specifies the corresponding output of that rule. Eq. , as given in Eq. (18). represents the final aggregated output of the fuzzy system, obtained by combining the contributions of all activated rules through a normalized weighted formulation.

Moreover, for lower associateship

$$\underline{N}_{\tilde{\mu}^m_{l|\overline{r}_t}} = \begin{cases} 1 - \left(\frac{a_l - J_{\tilde{\mu}_l^m}}{\underline{\Delta}_{\tilde{\mu}_l^m}}\right)^{\frac{1}{\overline{r}_t}} \text{ if } J_{\tilde{\mu}_l^m} - \underline{\Delta}_{\tilde{\mu}_l^m} < a_l \leq J_{\tilde{\mu}_l^m} \\ 1 - \left(\frac{a_l - J_{\tilde{\mu}_l^m}}{\overline{\Delta}_{\tilde{\mu}_l^m}}\right)^{\frac{1}{\overline{r}_t}} \text{ if } J_{\tilde{\mu}_l^m} < a_l \leq J_{\tilde{\mu}_l^l} + \overline{\Delta}_{\tilde{\mu}_l^m} \\ 0 \text{ if } a_l > J_{\tilde{\mu}_l^m} + \overline{\Delta}_{\tilde{\mu}_l^m} \text{ or } a_l \leq J_{\tilde{\mu}_l^m} - \underline{\Delta}_{\tilde{\mu}_l^m} \end{cases} \tag{19}$$

$$\underline{N}_{\tilde{\mu}^m_{l|\underline{r}_t}} = \begin{cases} 1 - \left(\frac{|a_l - J_{\tilde{\mu}_l^m}|}{\underline{\Delta}_{\tilde{\mu}_l^m}}\right)^{\frac{1}{\underline{r}_t}} \text{ if } J_{\tilde{\mu}_l^m} - \underline{\Delta}_{\tilde{\mu}_l^m} < a_l \leq J_{\tilde{\mu}_l^m} \\ 1 - \left(\frac{|a_l - J_{\tilde{\mu}_l^m}|}{\overline{\Delta}_{\tilde{\mu}_l^m}}\right)^{\frac{1}{\underline{r}_t}} \text{ if } J_{\tilde{\mu}_l^m} - < a_l \leq J_{\tilde{\mu}_l^m} + \overline{\Delta}_{\tilde{\mu}_l^m} \\ 0 \text{ if } a_l > J_{\tilde{\mu}_l^m} + \overline{\Delta}_{\tilde{\mu}_l^m} \text{ or } a_l \leq J_{\tilde{\mu}_l^m} - \underline{\Delta}_{\tilde{\mu}_l^m} \end{cases} \tag{20}$$

To improve the approximation capacity of a Type-3 fuzzy system, adaptive update laws are presented to adapt the rule parameters online through approximation error. The parameters are adapted such that they would minimize approximation error. This would help the system to learn the unknown nonlinear dynamics.

This adaptation process is designed to be compatible with the Lyapunov stability framework to keep the parameter estimations and the error terms bounded. When the system is combined with the MPC and LMI-based controller, it can remain stable to reach consensus in the presence of unknown dynamics, time delay, and cyber-physical attacks.

Where $\overline{N}_{\tilde{\mu}^m_{l|\overline{r}_t}}/\overline{N}_{\tilde{\mu}^m_{l|\underline{r}_t}}$ and $\underline{N}_{\tilde{\mu}^m_{l|\overline{r}_t}}/\underline{N}_{\tilde{\mu}^m_{l|\underline{r}_t}}$ are upper and lower associateship for $\tilde{\mu}^m_l$ at the levels of $\underline{r}_t$ and $\overline{r}_t$ where $J_{\tilde{\mu}^m_l}$ is the center of $J_{\tilde{\mu}^m_l}$ and $\underline{\Delta}_{\tilde{\mu}^m_l}$ and $\overline{\Delta}_{\tilde{\mu}^m_l}$ are the distances from the left point and the right point right of $J_{\tilde{\mu}^m_l}$ to $\tilde{\mu}^m_l$

Also in a Type-3 Fuzzy Logic System, the membership degree (associateship) of an input is not represented by a single value but instead by an interval bounded by upper and lower associateship functions, which capture higher-order uncertainty. The upper associateship function represents the maximum (optimistic) membership degree, while the lower associateship function represents the minimum (conservative) degree. These functions are defined based on the fuzzy set's center and spread, together with uncertainty parameters $\bar{r}_t$ and $\underline{r}_t$, which determine the width and shape of the membership curves. In particular, $\bar{r}_t$ corresponds to the upper uncertainty level and produces a wider, smoother membership function, whereas $\underline{r}_t$ corresponds to the lower uncertainty level and yields a narrower curve. These parameters satisfy $0 < \underline{r}_t < \bar{r}_t$, ensuring that the lower associateship always remains less than or equal to the upper associateship. Together, they form an uncertainty band that allows the Type-3 Fuzzy Logic System to effectively capture nonlinearities, noise, and disturbances, including sensor and actuator attacks in robotic and hydraulic systems.

3. The rules activating at $\underline{r}_t$, $\overline{r}_t$ are written as:

$$\overline{\Theta}^f_{\overline{r}_t} = \overline{N}_{\tilde{\mu}^{n_1}_{1|\overline{r}_t}} \,.\, \overline{N}_{\tilde{\mu}^{n_2}_{1|\overline{r}_t}} \;...\; \overline{N}_{\tilde{\mu}^{n_p}_{1|\overline{r}_t}}; \tag{21}$$

$$\overline{\Theta}^f_{\underline{r}_t} = \overline{N}_{\tilde{\mu}^{n_1}_{1|\underline{r}_t}} \,.\, \overline{N}_{\tilde{\mu}^{n_2}_{1|\underline{r}_t}} \;...\; \overline{N}_{\tilde{\mu}^{n_p}_{1|\underline{r}_t}}; \tag{22}$$

$$\underline{\Theta}^f_{\overline{r}_t} = \underline{N}_{\tilde{\mu}^{n_1}_{1|\overline{r}_t}} \,.\, \underline{N}_{\tilde{\mu}^{n_2}_{1|\overline{r}_t}} \;...\; \underline{N}_{\tilde{\mu}^{n_p}_{1|\overline{r}_t}}; \tag{23}$$

$$\underline{\Theta}^f_{\underline{r}_t} = \underline{N}_{\tilde{\mu}^{n_1}_{1|\underline{r}_t}} \,.\, \underline{N}_{\tilde{\mu}^{n_2}_{1|\underline{r}_t}} \;...\; \underline{N}_{\tilde{\mu}^{n_p}_{1|\underline{r}_t}}. \tag{24}$$

The $f-th$ rule is going to be.
$f-th$ rule:
If a_1 is $\tilde{\mu}^{n_1}_1$ and a_2 is $\tilde{\mu}^{n_2}_2$ and so on to a_p is $\tilde{\mu}^{n_p}_p$
Then

$$b \in [\underline{\zeta}_1 \;,\; \bar{\zeta}_1] \quad f = 1...N. \tag{25}$$

The rule parameters are denoted by a_l and $\underline{\zeta}_f$ and $\bar{\zeta}_f$ these are the inputs for $\tilde{\mu}^{n_m}_l$ which is the $n_m - th$ FS , which are enhanced.
$\underline{\zeta}_f$ and $\bar{\zeta}_f$ denote the lower and upper consequent parameters of the $f-th$ rule, respectively. Together, they define the interval $[\underline{\zeta}_f, \bar{\zeta}_f]$, which captures uncertainty in the rule output within the Type-3 fuzzy framework.
In a Type-3 Fuzzy Logic System, uncertainty is captured not only in the membership functions but also in the rule consequent. As a result, the output of each fuzzy rule is represented as an interval $[\underline{\zeta}_f, \bar{\zeta}_f]$, where $\underline{\zeta}_f$ and $\bar{\zeta}_f$ denote the lower and upper consequent parameters, respectively. This interval-based representation allows the system to account for higher-order uncertainty caused by nonlinear dynamics, external disturbances, and cyber-physical attacks. The overall system output is then obtained by aggregating the contributions of all rules across different uncertainty levels (cuts), using both the upper and lower firing strengths. The following equations describe this aggregation process.

4. Where the output is described as

$$b = \sum_{t=1}^{t}(\underline{r}_l\underline{b}_t + \overline{r}_t\bar{b}_t)/\sum_{t=1}^{t}(\underline{r}_t + \overline{r}_t). \tag{26}$$

Moreover,

$$\overline{b}_t = \frac{\sum_{f=1}^{p}(\overline{\Theta}^f_{\overline{r}_t}\overline{\zeta}_f + \underline{\Theta}^f_{\overline{r}_t}\underline{\zeta}_f)}{\sum_{f=1}^{p_s}(\overline{\Theta}^f_{\overline{r}_t} + \underline{\Theta}^f_{\overline{r}_t})}. \tag{27}$$

$$\underline{b}_t = \frac{\sum_{f=1}^{p_s}(\overline{\Theta}^f_{\underline{r}_t}\overline{\zeta}_f + \underline{\Theta}^f_{\underline{r}_t}\underline{\zeta}_f)}{\sum_{f=1}^{p_s}(\overline{\Theta}^f_{\underline{r}_t} + \underline{\Theta}^f_{\underline{r}_t})}. \tag{28}$$

Thus, the final output is computed as a normalized weighted average of the rule consequents, where both the upper and lower firing strengths jointly influence the decision-making process. This multi-level aggregation mechanism distinguishes the Type-3 fuzzy system from lower-order fuzzy models and strengthens its capability to represent complex and higher-order uncertainties. Where t and p_s denote the numbers of cuts and rules, respectively. Where h_l and k_l are the rule parameters of T3-FLSs these rule parameters are denoted by $\overline{\zeta}_{f_{hl}}/\underline{\zeta}_{f_{hl}}$ and $\overline{\zeta}_{f_{kl}}/\underline{\zeta}_{f_{kl'}}$ are improved then Eq. (29) is reduced as:

$$I = \frac{1}{2}\xi_l^2 = \frac{1}{2}(a_l - \widehat{a}_l)^2. \tag{29}$$

The cost function is defined in Eqs. (26) to (29) and is formulated using the same components as the Lyapunov–Krasovskii functional. It serves as an upper bound for the Lyapunov function over the prediction horizon. As a result, minimizing this cost function promotes a decrease in the Lyapunov function, and the inequality in Eq. (30) ensures the stability of the overall system.
Where the output of $l-th$ robots is a_l which is defined in Eq. (1) and $\widehat{a}_l$ is the approximation of a_l Eq. (2). Then $\overline{\zeta}_{f_{hl}}$ and $\overline{\zeta}_{f_{kl}}$ are renewed as.

$$\overline{\zeta}_{f_{hl}}(u+1) = \overline{\zeta}_{f_{hl}}(u) + \lambda\xi\frac{\sum_{t=1}^{t}\underline{r}_t}{\sum_{t=1}^{t}(\underline{r}_t + \overline{r}_t)}\frac{\overline{\Theta}^f_{\underline{r}_t}}{\sum_{f=1}^{p_s}(\overline{\Theta}^f_{\underline{r}_t} + \underline{\Theta}^f_{\underline{r}_t})} + \lambda\xi\frac{\sum_{t=1}^{t}\overline{r}_t}{\sum_{t=1}^{t}(\underline{r}_t + \overline{r}_t)}\frac{\overline{\Theta}^f_{\overline{r}_t}}{\sum_{f=1}^{p_s}(\overline{\Theta}^f_{\overline{r}_t} + \underline{\Theta}^f_{\overline{r}_t})}. \tag{30}$$

$$\begin{cases} \overline{\zeta}_{f_{kl}}(u+1) = \overline{\zeta}_{f_{kl}}(u) + \lambda\xi\frac{\sum_{u=1}^{t}\underline{r}_t}{\sum_{t=1}^{t}(\underline{r}_t+\overline{r}_t)}\frac{\overline{\Theta}^f_{\underline{r}_t}}{\sum_{f=1}^{p_s}(\overline{\Theta}^f_{\underline{r}_t}+\underline{\Theta}^f_{\underline{r}_t})}v_l(u)+ \\ \lambda\xi\frac{\sum_{t=1}^{t}\overline{r}_t}{\sum_{t=1}^{t}(\underline{r}_t+\overline{r}_t)}\frac{\overline{\Theta}^f_{\overline{r}_t}}{\sum_{f=1}^{p_s}(\overline{\Theta}^f_{\overline{r}_t}+\underline{\Theta}^f_{\overline{r}_t})}v_l(u) \end{cases} \tag{31}$$

Where λ is constant just for $\underline{\zeta}_{f_{hl}}$ and $\underline{\zeta}_{f_{kl}}$ we have

$$\underline{\zeta}_{f_{hl}}(u+1) = \underline{\zeta}_{f_{hl}}(u) + \lambda\xi\frac{\sum_{t=1}^{t}\underline{r}_t}{\sum_{t=1}^{t}(\underline{r}_t + \overline{r}_t)}\frac{\underline{\Theta}^f_{\underline{r}_t}}{\sum_{f=1}^{p_s}(\overline{\Theta}^f_{\underline{r}_t} + \underline{\Theta}^f_{\underline{r}_t})} + \lambda\xi\frac{\sum_{u=1}^{t}\overline{r}_t}{\sum_{t=1}^{t}(\underline{r}_t + \overline{r}_t)}\frac{\underline{\Theta}^f_{\overline{r}_t}}{\sum_{f=1}^{p_s}(\overline{\Theta}^f_{\overline{r}_t} + \underline{\Theta}^f_{\overline{r}_t})}. \tag{32}$$

The uncertainty set Ω represents all admissible uncertainties affecting the system, including fuzzy approximation errors, time-delay effects, and disturbances caused by sensor and actuator attacks. It is assumed that these uncertainties are bounded, i.e., $\Omega = \omega : |\omega| \leq \delta$. Where δ is a known positive constant. All variables and parameters involved in the optimization problem, including system states, control inputs, and uncertainty terms, are assumed to lie within this bounded set. This assumption ensures that the proposed min–max optimization problem is well-posed and effectively captures the worst-case system behavior in the presence of uncertainties.

$$\begin{cases} \underline{\zeta}_{f_{kl}}(u+1) = \underline{\zeta}_{f_{kl}}(u) + \lambda\xi\frac{\sum_{t=1}^{t}\underline{r}_t}{\sum_{t=1}^{t}(\underline{r}_t+\overline{r}_t)}\frac{\underline{\Theta}^f_{\underline{r}_t}}{\sum_{f=1}^{p_s}(\overline{\Theta}^f_{\underline{r}_t}+\underline{\Theta}^f_{\underline{r}_t})}v_l(u)+ \\ \lambda\xi\frac{\sum_{u=1}^{t}\overline{r}_t}{\sum_{t=1}^{t}(\underline{r}_t+\overline{r}_t)}\frac{\underline{\Theta}^f_{\overline{r}_t}}{\sum_{f=1}^{p_s}(\overline{\Theta}^f_{\overline{r}_t}+\underline{\Theta}^f_{\overline{r}_t})}v_l(u) \end{cases} \tag{33}$$

In a simplified form, it can be written as:

$$a(u) = \alpha_a(u) + \alpha_{ea}(u-e) + \gamma v_2(u). \tag{34}$$

Where $a(u) = [a_1^\tau(u)...a_w^\tau(u)]^\tau \in \mathbb{R}^{pw}, a(u-e) = [a_1^\tau(u-e)...a_w^\tau(u-e)]^\tau \in \mathbb{R}^{pw}$ and $v^2(u) = [v_{21}^\tau(u), ..., v_{2w}^\tau(u)]^\tau \in \mathbb{R}^{qw}$.

$$\alpha = \begin{bmatrix} \alpha_1 & 0 & \cdots & 0 \\ 0 & \alpha_2 & \vdots & 0 \\ \vdots & \vdots & \ddots & \vdots \\ 0 & 0 & \cdots & \alpha_w \end{bmatrix}_{pw\times pw} \qquad \alpha_e = \begin{bmatrix} \alpha_{e1} & 0 & \cdots & 0 \\ 0 & \alpha_{e2} & \vdots & 0 \\ \vdots & \vdots & \ddots & \vdots \\ 0 & 0 & \cdots & \alpha_{ew} \end{bmatrix}_{pw\times pw} \qquad \gamma = \begin{bmatrix} \gamma_1 & 0 & 0 & \cdots & 0 \\ 0 & \gamma_2 & \vdots & \vdots & 0 \\ \vdots & \vdots & \ddots & \ddots & \vdots \\ 0 & 0 & \cdots & \cdots & \gamma_w \end{bmatrix}_{pw\times qw} \tag{35}$$

Using Eq. 10, the new vector is further given by:

$$d(u) = [d_1^\tau(u)...d_w^\tau(u)]^\tau \in \mathbb{R}^{pw}.$$

$$d(u) = a(u) - \frac{1}{w}(\phi \otimes \iota_p)a(u) = \left(\iota - \frac{1}{w}(\phi \otimes \iota_p)\right) a(u). \tag{36}$$

Eq. 36 defines the consensus error vector by mapping the system states into an error coordinate system. This transformation is essential for constructing the Lyapunov–Krasovskii functional, as it enables the stability analysis to be carried out on the consensus error dynamics instead of the original system states.
According to Eq. 34 and Eq. 36 the equation becomes:

$$d(u+1) = \left(\iota - \frac{1}{w}(\phi \otimes \iota_p)\right) a(u+1)$$

$$= \left(\iota - \frac{1}{w}(\phi \otimes \iota_p)\right) \alpha_a(u) + \left(\iota - \frac{1}{w}(\phi \otimes \iota_p)\right) \alpha_{ea}(u-e) + \left(\iota - \frac{1}{w}(\phi \otimes \iota_p)\right) \gamma v_2(u).$$

$$\alpha^j a(u) + \alpha_e^j a(u-e) + \gamma^j v_2(u). \tag{37}$$

Where:

$$\alpha^j = \begin{bmatrix} \alpha_1 & -\frac{\phi_{12}}{w}\alpha_2 & \cdots & -\frac{\phi_{1w}}{w}\alpha_w \\ -\frac{\phi_{21}}{w}\alpha_1 & \alpha_2 & \vdots & \vdots \\ \vdots & \vdots & \ddots & \vdots \\ -\frac{\phi_{w1}}{w}\alpha_1 & -\frac{\phi_{w2}}{w}\alpha_2 & \cdots & \alpha_w \end{bmatrix}_{pw\times pw}$$

$$\alpha_e^j = \begin{bmatrix} \alpha_{e1} & -\frac{\phi_{12}}{w}\alpha_{e2} & \cdots & -\frac{\phi_{1w}}{w}\alpha_{ew} \\ -\frac{\phi_{21}}{w}\alpha_{e1} & \alpha_{e2} & \vdots & \vdots \\ \vdots & \vdots & \ddots & \vdots \\ -\frac{\phi_{w1}}{w}\alpha_{e1} & -\frac{\phi_{w2}}{w}\alpha_{e2} & \cdots & \alpha_{ew} \end{bmatrix}_{pw\times pw}$$

$$\gamma^j = \begin{bmatrix} \gamma_1 & -\frac{\phi_{12}}{w}\gamma_2 & -\frac{\phi_{13}}{w}\gamma_3 & \cdots & -\frac{\phi_{1w}}{w}\gamma_w \\ -\frac{\phi_{21}}{w}\gamma_1 & \gamma_2 & \vdots & \vdots & \vdots \\ \vdots & \vdots & \ddots & \ddots & \vdots \\ -\frac{\phi_{w1}}{w}\gamma_1 & -\frac{\phi_{w2}}{w}\gamma_2 & \cdots & \cdots & \gamma_w \end{bmatrix}_{pw\times qw} \tag{38}$$

From Eq. 36 we get:

$$d(u) = \left(\iota - \frac{1}{w}(\phi \otimes \iota_p)\right) a(u).$$

$$\to a(u) = \left(\iota - \frac{1}{w}(\phi \otimes \iota_p)\right)^{-1} d(u). \tag{39}$$

Put Eq. 39 into Eq. 37 we get:

$$d(u+1) = \alpha^j \left(\iota - \frac{1}{w}(\phi \otimes \iota_p)\right)^{-1} d(u) + \alpha_e^j \left(\iota - \frac{1}{w}(\phi \otimes \iota_p)\right)^{-1} d(u-e) + \gamma^j v_2(u).$$

$$\widehat{\alpha}^j d(u) + \widehat{\alpha}_e^j d(u-e) + \gamma^j v_2(u). \tag{40}$$

This work studies a multi-robot network with nonlinear, time-delayed dynamics under uncertainties and cyber-attacks. Unknown dynamics are approximated using a Type-3 Fuzzy Logic System with adaptive learning to improve robustness over lower-order fuzzy methods. A consensus-based control strategy is developed to achieve coordinated formation despite approximation errors, sensor/actuator attacks, and communication delays. Stability and convergence are ensured using a Lyapunov-based Model Predictive Control framework with Min–Max optimization via Linear Matrix Inequalities. As shown in Fig. (2), the proposed method achieves secure and stable multi-robot coordination under adverse conditions.

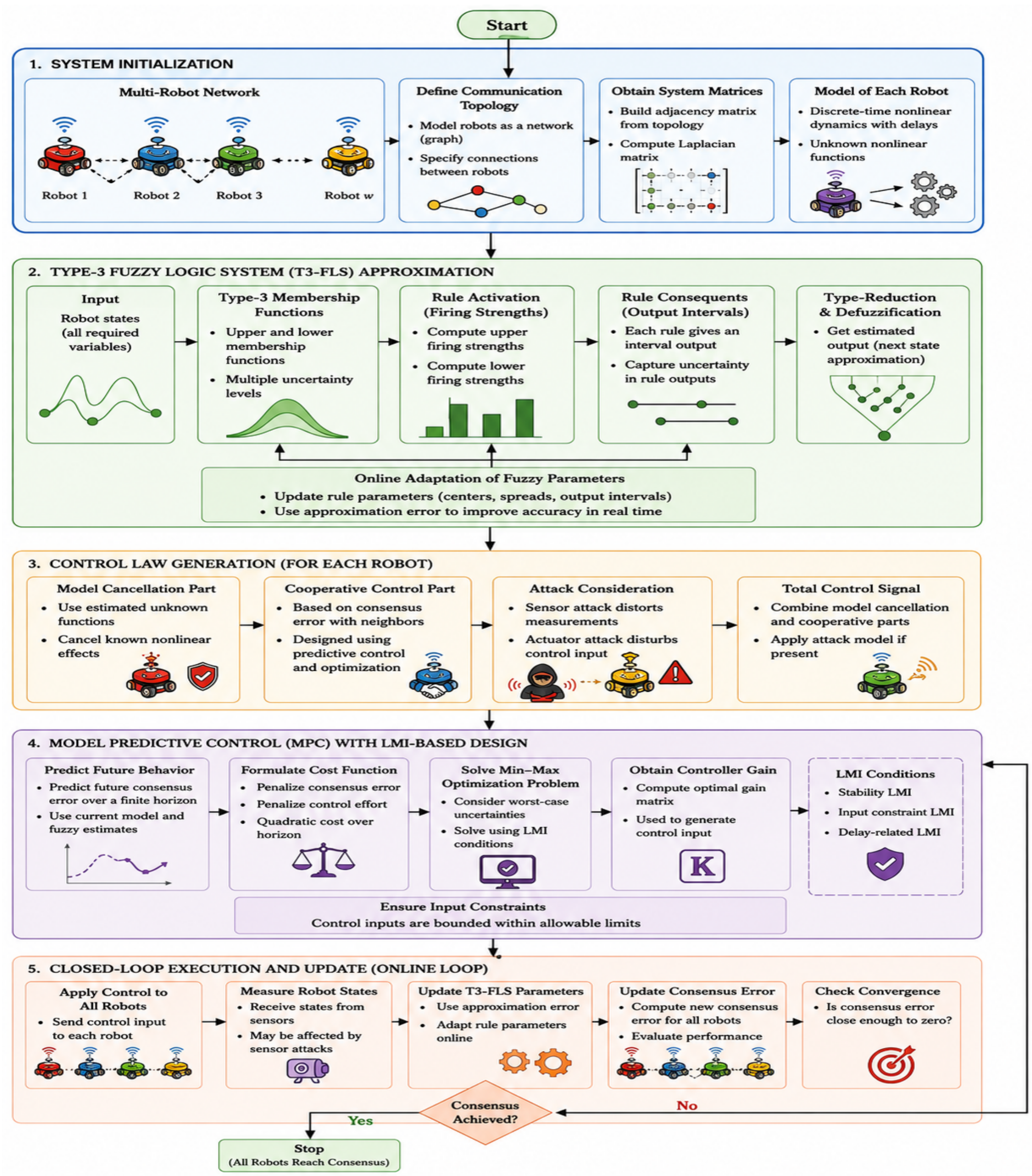

Figure 2: Secure cooperative multi-robot formation with adaptive coordination under attacks and delays.

Remark 4.1. *Although higher-type fuzzy systems (e.g., Type-3) offer stronger capability for handling uncertainties, performance improvements can also be achieved by optimizing the fuzzy inference structure. In particular, refining the rule base, tuning the membership functions, and incorporating adaptive learning mechanisms can significantly improve approximation accuracy without increasing the fuzzy system type. This provides an effective trade-off between computational complexity and control performance, since lower-type fuzzy systems with well-optimized inference structures may* *achieve comparable results with a reduced computational burden.*

4.7 Type-3 fuzzy logic system formulation

A Type-3 fuzzy logic system (T3-FLS) is employed to handle higher-order uncertainties and nonlinear disturbances in the multi-agent system. Unlike Type-1 and Type-2 fuzzy systems, a Type-3 fuzzy set introduces uncertainty in the membership grades themselves. Let the input vector be defined as $z(t) \in \mathbb{R}^n$. The T3-FLS is constructed using a set of fuzzy rules of the form: **Rule** i**:** If z_1 is $\tilde{F}_{i1}$ and $\cdots$ and z_n is $\tilde{F}_{in}$, then

$$y_i = g_i(z), \tag{41}$$

where $\tilde{F}_{ij}$ denotes Type-3 fuzzy sets.
The Type-3 membership function is expressed as an interval-valued uncertainty:

$$\mu_{\tilde{F}}(x) = [\underline{\mu}(x), \overline{\mu}(x)]. \tag{42}$$

The final fuzzy output is obtained through type-reduction and defuzzification as:

$$y(t) = \sum_{i=1}^{N} w_i(z(t))\, y_i, \tag{43}$$

where the normalized firing strength is defined as:

$$w_i(z) = \frac{\mu_i(z)}{\sum_{j=1}^{N} \mu_j(z)}. \tag{44}$$

The T3-FLS is used to approximate the nonlinear control law and compensate uncertainties in the system as:

$$v_2(u) = F_{T3}(d(u)), \tag{45}$$

where $F_{T3}(\cdot)$ represents the fuzzy inference mapping.

5 Model predictive control

Suppose that the estimated control signals of robots, considering the prediction x, are

$$||v_{2l}(u + x|u)||_2 \leq \overline{v}_{2l} \quad l = 1, 2, ..., w. \tag{46}$$

The cost function with infinite prospects for the robot l is represented as:

$$G_l(u) = \sum_{x=0}^{\infty} d_l^{\tau}(u + x|u) Y_d d_l(u + x|u) + v_{2l}^{\tau}(u + x|u) Y_v v_{2l}(u + x|u). \tag{47}$$

Where $Y_d = Y_d^{\tau}$ and $Y_v = Y_v^{\tau}$ are positive-definite matrices.
Lastly, as one:

$$||v_2(u + x|u)||_2 \leq \overline{v}_2 \quad \overline{v}_2 = \sum_{l=1}^{w} \overline{v}_{2l}. \tag{48}$$

To determine the predictive controller satisfying Eq. 48, an the infinite prospect function is proposed.

$$G(U) = \sum_{x=0}^{\infty} d^{\tau}(u + x|u) \widehat{Y}_d d(u + x|u) + v_2^{\tau}(u + x|u) \widehat{Y}_v v_2(u + x|u). \tag{49}$$

The MPC cost function is formulated in quadratic form in terms of the state error and control input, consistent with the structure of the Lyapunov–Krasovskii functional used for stability analysis. With appropriately chosen weighting matrices, the cost function can be interpreted as an upper bound of the Lyapunov function. Therefore, minimizing the MPC objective leads to a decrease in the Lyapunov function over time, thereby ensuring the stability of the closed-loop system.

Where $\widehat{Y}_d = diag\{Y_d, Y_d, ..., Y_d\} \in \mathbb{R}^{pw\times pw}$ and $\widehat{Y}_v = diag\{Y_v, Y_v, ..., Y_v\} \in \mathbb{R}^{qw\times qw}$ are steady weighting matrices.Thus, the cost function takes the following form."

$$G(u) = G_1(u) + G_2(u) + ... + G_w(u). \tag{50}$$

Suppose we minimize $G(u)$. In that case, the result we get by minimizing it is $G_l(u), \quad l = 1, 2, ..., w$.
An upper limit is also intended to minimize the specified cost function and, by extension, the cost function is minimized using the upper limit.
Where ρ is determined by the Lyapunov-Krasovski method:

$$\rho(u+x+1|u) - \rho(u+x|u) \leq -[d^\tau(u+x|u)Y_d d(u+x|u) + v_2^\tau(u+x|u)Y_v v_2(u+x|u)]. \tag{51}$$

Using Eq. 51, we can write:

$$\sum_{x=0}^{\infty}\rho(u+x+1|u) - \rho(u+x|u) \leq -\sum_{x=0}^{\infty}[d^\tau(u+x|u)Y_d d(u+x|u) + v_2^\tau(u+x|u)Y_v v_2(u+x|u)]. \tag{52}$$

The expression on the right of Eq. 52 denotes the infinite-term quadratic cost function, projected in Eq. 49, then the expression on the left of Eq. 52 can be reduced to:

$$\rho(\infty) - \rho(u) \leq -G(t). \tag{53}$$

Hence, inequality 53 results in $G(u) < \rho(u)$, and the efficiency problem of minimizing $G(u)$ can be obtained.
The optimization problem will be solved using the Min-Max method. In the worst case, the cost function gets the maximum value because it is maximized. The following procedure is used to solve the Min-Max problem.

$$\min_{V(u+x|u)}\left(\max_{[\breve{\alpha}(u+x)\widehat{\gamma}(u+x)\alpha^e(\breve{u}+x)\in\overline{\Omega}]} \mathrm{I(u)}\right). \tag{54}$$

$\overline{\Omega}^l$ is the convex polyhedron of $l-th$ robots. Moreover, the control vector amplitudes of the robots are bounded such that.

$$||v^l(u+x|u)||_2 \leq v^l_{max} \ for \ l = 1, 2...w. \tag{55}$$

Where v^l_{max} are positive constants; accordingly, the following equation can be derived.

$$||V_2(u+x|u)||_2 \leq \overline{v}_{max}. \tag{56}$$

Where $\overline{v}_{max} = \sum_{l=1}^{w} v^l_{max}$. The following theorem provides enough conditions for $v_2(u+x|u); x \geq 0$ to develop the controller developed from linear matrix inequalities along with the idea of asymptotic stability of Eq. 40. Also, the matrices A, B, and C obtained from the LMI conditions are used to design the controller. The controller gain is then determined after solving the LMI conditions. In the proposed approach, the LMIs are formulated in terms of decision matrices that guarantee system stability and performance. Once the LMIs are feasible, these matrices are obtained numerically using standard optimization solvers. The controller gain is then constructed from the computed matrices, typically by multiplying one decision matrix by the inverse of another. This ensures that the resulting controller satisfies the Lyapunov-based stability conditions. In particular the control gain is defined as $\xi = CA^{-1}$, which directly determines the control law $v_2(u) = \xi d(u)$. This provides a direct link between the LMI-based stability conditions and the implemented controller.

Note: The main goal of the proof can be described briefly to enhance clarity. The construction of the Lyapunov-Krasovskii functional guarantees that the consensus error will decay asymptotically. The inequality thus obtained is then reduced and reformulated in terms of LMIs.

Theorem 5.1. *Observe Eq. (40) using the control law* $v_2(u) = \xi d(u)$. *That reduces the cost of the function Eq. (49). When there are matrices* $0 < A = A^\tau \in \mathbb{R}^{pw\times pw}$, $C \in \mathbb{R}^{qw\times pw}$, *and* $0 < B = B^\tau \in \mathbb{R}^{pw\times pw}$ *and scalar* $\lambda > 0$, *so that the following LMIs and optimization problem are solvable.*

$$\min_{subject\ to} \lambda\ . \tag{57}$$

$$\begin{bmatrix} \overline{v}^2_{max}\iota_{N\times N} & C \\ C^\tau & A \end{bmatrix} > 0. \tag{58}$$

$$\begin{bmatrix} A & C^\tau(\widehat{Y}_v)^{(\frac{1}{2})} & A(\widehat{Y}_d)^{(\frac{1}{2})} & A & 0 & (\widehat{\alpha}^j A+\gamma^j C)^\tau \\ * & \lambda^\iota & 0 & 0 & 0 & 0 \\ * & * & \lambda^\iota & 0 & 0 & 0 \\ * & * & * & B & 0 & 0 \\ * & * & * & * & B & (\widehat{\alpha}_e^j)^\tau \\ * & * & * & * & * & A \end{bmatrix} > 0. \tag{59}$$

$$\begin{bmatrix} 1 & d^\tau(u) & d^\tau(u-1) & \cdots & d^\tau(u-e) \\ * & A & 0 & \cdots & 0 \\ * & * & B & \cdots & 0 \\ \vdots & \vdots & \vdots & \ddots & \vdots \\ * & * & * & \cdots & B \end{bmatrix} > 0. \tag{60}$$

This leads to $\xi = CA^{-1} \in \mathbb{R}^{qw\times pw}$ to achieve consensus.

Proof. Consider the following Lyaunov-Krasovskii functional,

$$\rho(d(u)) = d(u)^\tau P d(u) + \sum_{q=u-e}^{u-1} d(q)^\tau Q d(q) = \rho_1(d(u)) + \rho_2(d(u)). \tag{61}$$

Where P and Q are Matrices containing only positive values. The delay value affects the number of terms of $\rho_2(d(u))$. Consider the Lyapunov-Krasovskii functional satisfying the following relation.

$$\rho(d(u+x+1|u)) - \rho(d(u+x|u)) \leq -[d(u+x|u)^\tau \tilde{Y}_d d(u+x|u)) + v_2(u+x|u)^\tau \tilde{Y}_v v_2(u+x|u)]. \tag{62}$$

If we sum both sides of the above inequality from $x = 0$ to ∞, we get

$$\sum_{x=0}^{\infty}[\rho(d(u+x+1|u)) - \rho(d(u+x|u))] \leq -\sum_{x=0}^{\infty}[d(u+x|u)^\tau \tilde{Y}_d d(u+x|u) + v_2(u+x|u)^\tau \tilde{Y}_v v_2(u+x|u)]. \tag{63}$$

After simplifying the left side, we obtain:

$$\rho(d(\infty)) - \rho(d(u)) \leq -I(u). \tag{64}$$

According to the asymptotic convergence of $d(u)$, then $\lim_{u\to\infty} d(u) = 0$and therefore $\rho(d(\infty)) = 0$.
So one has.

$$-\rho(d(u)) \leq -I(u). \tag{65}$$

Also

$$I(u) \leq \rho(d(u)). \tag{66}$$

Therefore,

$$\left(\max_{[\check{\alpha}(u+x)\widehat{\gamma}(u+x)\check{\alpha}^e(u+x)]\in\overline{\Omega}} \text{I(u)} \right). \\ \leq \rho(d(u)).$$

And it can be resolved as the function $\rho(d(u))$ is an upper limit for the cost function $I(u)$. Then the Minimum and the maximum problem Eq. (54) may be rewritten as $\rho(d(u))$ as given below.

$$\min_{v(u+x|u)} \rho(d(u)). \tag{67}$$

The upper limit of the Lyapunov-Krasovskii functional $\rho(d(u))$ complies with Eq. (68) for some constant greater than zero λ

$$\rho(d(u)) \leq \lambda. \tag{68}$$

The LMI conditions are obtained by constructing a Lyapunov–Krasovskii functional and evaluating its forward difference along the system trajectory. The resulting expression is then upper-bounded using standard inequality techniques to manage cross terms and time-delay-related components. By reorganizing the terms into a quadratic form, a matrix inequality is established. This condition is subsequently converted into an LMI through the application of the Schur

complement. Finally, the controller gain is computed directly from the feasible LMI solution, which guarantees the stability and convergence of the closed-loop system.
Accordingly, the Maximization or minimization problem Eq. (67) can be rewritten as the following optimization problem. Now regarding relations Eq. (61) and Eq. (68), it is expressed as

$$d(u)^\tau P d(u) + \sum_{q=u-e}^{u-1} d(q)^\tau Q d(q) \leq \lambda. \tag{69}$$

Establishing the following definitions.

$$A^{-1} = \lambda^{-1} P B^{-1} = \lambda^{-1} Q. \tag{70}$$

Then, Eq. (69) yields

$$1 - d(u)^\tau A^{-1} d(u) - d(u-1)^\tau B^{-1} d(u-1) - \cdots - d(u-e)^\tau B^{-1} d(u-e) \geq 0. \tag{71}$$

By applying a standard matrix inequality transformation based on the Schur complement, the inequality in (71) is equivalently expressed as

$$\begin{bmatrix} 1 & d^\tau(u) & d^\tau(u-1) & \cdots & d^\tau(u-e) \\ * & A & 0 & \cdots & 0 \\ * & * & B & \cdots & 0 \\ \vdots & \vdots & \vdots & \ddots & \vdots \\ * & * & * & \cdots & B \end{bmatrix} > 0. \tag{72}$$

Hence, LMI Eq. (60) is attained. The outcome of e affects the above LMI dimension
Now, regarding the Lyapunov-Krasovskii functional, the time derivative of $\rho(d(u))$ equals.

$$\Delta\rho(d(u)) = \Delta\rho_1(d(u)) + \Delta\rho_2(d(u)). \tag{73}$$

And $(x+1)th$ step of $\Delta\rho(d(u))$ is

$$\Delta\rho(d(u+x|u)) = \Delta\rho_1(d(u+x|u)) + \Delta\rho_2(d(u+x|u)). \tag{74}$$

The inequality in Eq. (62) is equivalent to the following relation:

$$(-\nu^\tau \Lambda \nu) < 0 \quad for \quad \nu \neq 0. \tag{75}$$

Where

$$\nu^\tau = [d(u+x|u)^\tau \quad d(u+x-e|u)^\tau]. \tag{76}$$

$$\Lambda = \begin{bmatrix} \Xi_{11} & \Xi_{12} \\ \Xi_{21} & \Xi_{22}. \end{bmatrix} \tag{77}$$

And

$$\begin{aligned} \Xi_{11} &= -\alpha^r(u+x)^\tau P \alpha^r(u+x) = P - Q - \tilde{Y}_d - F^\tau Y_v F. \\ \Xi_{12} &= -\alpha^r(u+x)^\tau P \breve{\alpha}^e(u+x). \\ \Xi_{21} &= -\breve{\alpha}^e(u+x)^\tau P \alpha^r(u+x). \\ \Xi_{22} &= -\breve{\alpha}^e(u+x)^\tau P \breve{\alpha}^e(u+x). \end{aligned} \tag{78}$$

Where

$$\alpha^r(u+x) = (\breve{\alpha}(u+x) + \widehat{\gamma}(u+x)F).$$

Inequality Eq. (73) is obtained if $\Lambda > 0$, now considering the definitions given below.

$$A^{-1} = \lambda^{-1} P B^{-1} = \lambda^{-1} Q F A = C. \tag{79}$$

The inequality $\Lambda > 0$ corresponds to the following relation:

$$\begin{bmatrix} -\alpha^r(u+x)^\tau A^{-1} \alpha^r(u+x) + A^{-1} - B^{-1} - \lambda^{-1}\tilde{Y}_d - \lambda^{-1} F^\tau \tilde{Y}_v F & -\alpha^r(u+x)^\tau A^{-1} \breve{\alpha}^e(u+x) \\ -\breve{\alpha}^e(u+x)^\tau A^{-1} \alpha^r(u+x) & -\breve{\alpha}^e(u+x)^\tau A^{-1} \breve{\alpha}^e(u+x) + B^{-1} \end{bmatrix} > 0. \tag{80}$$

It is observed that the above inequality is not in LMI form. By applying appropriate inequality transformations twice, the following LMI form is obtained:

$$\begin{bmatrix} A^{(-1)} - B^{(-1)} - \lambda^{(-1)}\tilde{Y}_d - \lambda^{(-1)}F^\tau \tilde{Y}_v F & 0 & (\alpha^r(u+x)^)\tau \\ * & B & (\check{\alpha}^e(u+x))^\tau \\ * & * & A \end{bmatrix} > 0. \tag{81}$$

The operator by $diag(A, \iota, \iota)$ denotes block diagonal multiplication, i.e., pre-multiplication and post-multiplication of the matrix inequality by $diag(A, \iota, \iota)$, where ι is the identity matrix. This operation preserves symmetry and is used to transform the inequality into an equivalent LMI form. Left- and right-multiplying the equation by $diag(A, \iota, \iota)$ results in

$$\begin{bmatrix} A - AB^{(-1)}A - A\lambda^{(-1)}\tilde{Y}_d A - \lambda^{(-1)}C^\tau \tilde{Y}_v C & 0 & (\check{\alpha}(u+x)A + \widehat{\gamma}(u+x)C)^\tau \\ * & B & (\check{\alpha}^e(u+x))^\tau \\ & * & A \end{bmatrix} > 0. \tag{82}$$

Now, considering $\tilde{Y}_v = \tilde{Y}_v^{\frac{1}{2}} \tilde{Y}_v^{\frac{1}{2}}$ and $\tilde{Y}_d = \tilde{Y}_d^{\frac{1}{2}} \tilde{Y}_d^{\frac{1}{2}}$, Eq. (82) can be rewritten as:

$$\begin{bmatrix} A & C^\tau \tilde{Y}_v^{\frac{1}{2}} & A\tilde{Y}_d^{\frac{1}{2}} & A & 0 & (\check{\alpha}(u+x)A + \widehat{\gamma}(u+x)C)^\tau \\ * & \lambda\iota & 0 & 0 & 0 & 0 \\ * & * & \lambda\iota & 0 & 0 & 0 \\ * & * & * & B & 0 & 0 \\ * & * & * & * & B & (\check{\alpha}^e(u+x))^\tau \\ * & * & * & * & * & A \end{bmatrix} > 0. \tag{83}$$

The matrices $\check{\alpha}(u+x), \check{\gamma}(u+x)$ and $\check{\alpha}^e(u+x)$ contain polytopic uncertainties, meaning the above inequality cannot be solved because the polytopic sets have a convexity characteristic. It depends on the number of vertices of $\overline{\Omega}$. The expression of the above inequality is as follows.

$$\begin{bmatrix} A & C^\tau \tilde{Y}_v^{\frac{1}{2}} & A\tilde{Y}_d^{\frac{1}{2}} & A & 0 & (\check{\alpha}_j A + \widehat{\gamma}_j C)^\tau \\ * & \lambda\iota & 0 & 0 & 0 & 0 \\ * & * & \lambda\iota & 0 & 0 & 0 \\ * & * & * & B & 0 & 0 \\ * & * & * & * & B & (\check{\alpha}_j^e)^\tau \\ * & * & * & * & * & A \end{bmatrix} > 0. \tag{84}$$

Hence, LMI Eq. (59) is attained. At this point, an invariant set must be defined to satisfy the LMI. 58, due to the limitations on input amplitudes. Considering $\rho(d(u)) \leq \lambda$ for all $u \in [0, \infty)$, therefore

$$\rho(d9u + x|u)) = d(u+x)^\tau P d(u+x) + \sum_{q=u+x-e}^{u+x-1} d(q)^\tau Q d(q) \leq \lambda. \tag{85}$$

Considering relation Eq. (70) one has

$$d(u+x|u)^\tau A^{-1} d(u+x|u) + \sum_{q=u+x-e}^{u+x-1} d(q)^\tau B^{-1} d(q) \leq 1. \tag{86}$$

$$d(u+x|u)^\tau A^{-1} d(u+x|u) \leq 1. \tag{87}$$

Therefore, the following invariant set is defined

$$\psi = \{d(u) | d^\tau(u) A^{-1} d(u) \leq 1\}. \tag{88}$$

Now considering $v_2(u+x|u) = Fd(u+x|u) = CA^{-1}d(u+x|u)$ Eq. (56) becomes

$$\begin{aligned} ||v_2(u+x|u)||_2^2 = ||CA^{-1}d(u+x|u)||_2^2 &= d^\tau(u+x|u)A^{-\frac{1}{2}}A^{-\frac{1}{2}}C^\tau CA^{-\frac{1}{2}} \times A^{-\frac{1}{2}}d(u+x|u) \\ &\leq \Gamma_{max}(A^{-\frac{1}{2}}C^\tau CA^{-\frac{1}{2}}) \times ||A^{-\frac{1}{2}}d(u+x|u)||_2^2 \leq \overline{v}_{max}^2. \end{aligned} \tag{89}$$

Because $d(u) \in \psi$ one has $||A^{-\frac{1}{2}}d(u+x|u)||_2^2 \leq 1$ and then the above inequality is reduced to

$$\begin{aligned} &\Gamma_{max}(A^{-\frac{1}{2}}C^{\tau}CA^{-\frac{1}{2}}) \leq \overline{v}_{max}^2. \\ &\Rightarrow A^{-\frac{1}{2}}C^{\tau}CA^{-\frac{1}{2}} \leq \overline{v}_{max}^2\iota. \\ &\overline{v}_{max}^2\iota - A^{-\frac{1}{2}}C^{\tau}CA^{-\frac{1}{2}} \geq 0. \end{aligned} \tag{90}$$

Multiplying the equation on both sides by $A^{\frac{1}{2}}$, the following inequality can be written as

$$\begin{bmatrix} \overline{V}_{max}^2\iota_{N\times N} & C \\ C^{\tau} & A \end{bmatrix} > 0. \tag{91}$$

Accordingly, the inequality in Eq. (58) is obtained, completing the proof. □

Remark 5.2. *In practical implementation, the proposed control structure combines LMI-based state feedback with a Type-3 fuzzy logic system. The fuzzy system provides adaptive compensation in the presence of nonlinear uncertainties and external disturbances that are not captured by the linear model.*
The overall control law is implemented as:

$$v_2(u) = \xi d(u) + F_{T3}(d(u)), \tag{92}$$

where $\xi d(u)$ guarantees stability and convergence, while $F_{T3}(d(u))$ enhances robustness. The LMI conditions ensure that the closed-loop system remains asymptotically stable even under bounded fuzzy uncertainty.

Note: From the above, the consensus error is decreasing over time, hence the system remains stable. The LMI method provides an easy technique for calculating the controller gain.

Remark 5.3. *Raising the number of robots is unable to pose an equation for the suggested methodology. At the same time, it simply expands the LMIs' dimension given in Theorem (5.1), which is solvable using software tools. To verify the assumptions of Theorem (5.1), the proposed conditions are formulated as a set of LMIs, which can be solved numerically using standard convex optimization tools. In particular, the matrices A, B, and C are treated as decision variables, and the feasibility of inequalities Eq. (58–60) is tested using software such as MATLAB (YALMIP or the LMI Toolbox). If a feasible solution is obtained, the assumptions are satisfied, and the controller gain $\xi = CA^{-1}$ can then be computed accordingly.*

In addition, the proposed architecture is scalable to the number of robots. Expanding the size of the network does not affect the controller structure, apart from expanding the dimensions of the LMI constraints. As long as the LMI conditions maintain their convex nature, they are solvable using efficient techniques.

Derivation of LMI Conditions

- We start from the consensus error model in Eq. 40 and select a Lyapunov–Krasovskii function to study stability. The goal is to ensure that this function decreases over time.
- By substituting the system dynamics into the Lyapunov function, an inequality is obtained that depends on the current state, delayed state, and control input.
- The resulting expression contains cross terms (products of variables), which are difficult to handle directly.
- These cross terms are bounded using standard techniques so that they can be written in a simpler form without variable multiplication.
- The inequality is then rewritten in matrix form using the system matrices defined earlier.
- New matrix variables are introduced to simplify the expression and make it linear in the unknowns.
- The Schur complement is applied to convert the inequality into a standard LMI form.
- Finally, all conditions are combined into a single matrix inequality that can be solved using LMI tools. If this condition is satisfied, the system is stable, and the control gain can be obtained.

5.1 Computational complexity and real-time implementation

Computational Complexity and Real-Time Implementation: The main computational burden associated with the suggested scheme relates to the Type-3 fuzzy inference and MPC algorithm. Fuzzy inference complexity is of order $O(N.p.t)$, where N stands for the number of rules and t is the number of different uncertainty levels. To speed up computations, a concise rule base will be considered. The LMI-based optimization problem is calculated beforehand, while the controller gain is computed online. Moreover, MPC uses a finite prediction horizon; hence, the computational time is finite as well.

6 Simulation results

The suggested approach is also compared with the standard MPC, LQR, and SMC approaches under the same circumstances for a thorough comparison.
In the following section, a nonlinear multi-robotic system and a Duffing-Holmes chaotic system are used to assess the impact of the control approach. Derived from the MPC method and suggests a Type-3 fuzzy system. Detailed examinations are indicated when computer simulations are performed. By selecting design parameters, we can analyze the feasibility of the Theorem (5.1).

Example 6.1. *The network of four robots that are connected by following the adjacency matrix, whose communication topology is represented in Figure (3).*

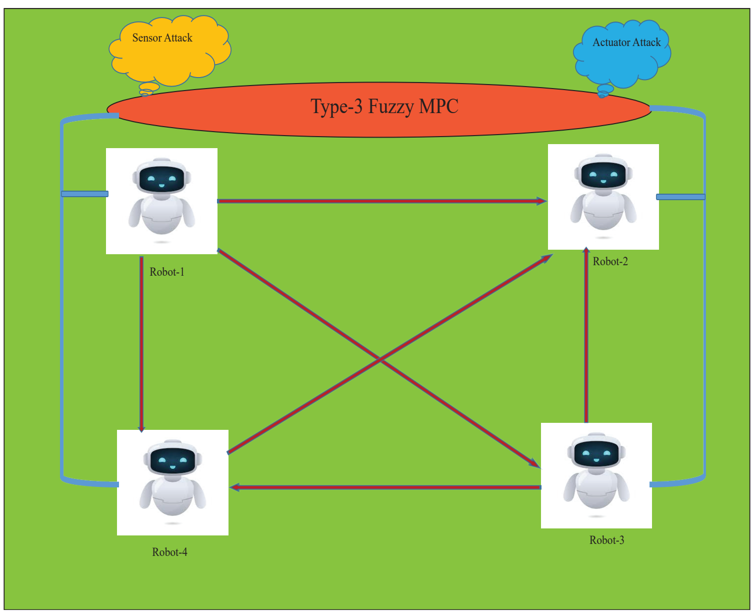

Figure 3: Communication Topology of Robots.

$$\phi = \begin{bmatrix} \vartheta_{11} & \vartheta_{12} & \vartheta_{13} & \vartheta_{14} \\ \vartheta_{21} & \vartheta_{22} & \vartheta_{23} & \vartheta_{24} \\ \vartheta_{31} & \vartheta_{32} & \vartheta_{33} & \vartheta_{34} \\ \vartheta_{41} & \vartheta_{42} & \vartheta_{43} & \vartheta_{44} \end{bmatrix} = \begin{bmatrix} 0 & 1 & 1 & 1 \\ 0 & 0 & 1 & 1 \\ 0 & 0 & 0 & 1 \\ 0 & 0 & 0 & 0 \end{bmatrix}. \tag{93}$$

The corresponding Laplacian matrix $\mathcal{L} = \mathcal{D} - \mathcal{A}$ is,

$$\mathcal{L} = \begin{bmatrix} 3 & -1 & -1 & -1 \\ 0 & 2 & -1 & -1 \\ 0 & 0 & 1 & -1 \\ 0 & 0 & 0 & 0 \end{bmatrix}.$$

From Eq. (1), the dynamics of robots are contemplated as a Duffing-Holmes chaotic system

$$\begin{cases} \dot{a}_{l1} = a_{l2} \\ \dot{a}_{l2} = -\frac{1}{2.5^2}a_{l1}^3 - a_{l1} - 0.1a_{l2} + 0.025a_{l1}(u-T) \\ +0.025a_{l1}^2(u-T) + 0.01a_{l2}(u-T) + 62.5\cos(1.29u) \end{cases} \tag{94}$$

It is known that the Duffing-Holmes chaotic system is a type of chaotic behavior in which its dynamics are sensitive to initial conditions, which can give unpredictable results. So the minor modifications in the initial condition of chaotic followers cause significant variations in the system's dynamics. The networked control policies which are utilized in the system are as follows

$$\begin{aligned} v_{11}(u) &= \widehat{k}_1^{-1}(a_1(u), \mu_{k1}(u))[-\widehat{h}_1(a_1(u), \mu_{n1}(u)) + \alpha_1 a_1(u)], \\ v_{12}(u) &= \widehat{k}_2^{-1}(a_2(u), \mu_{k2}(u))[-\widehat{h}_2(a_2(u), \mu_{n2}(u)) + \alpha_2 a_2(u)], \\ v_{13}(u) &= \widehat{k}_3^{-1}(a_3(u), \mu_{k3}(u))[-\widehat{h}_3(a_3(u), \mu_{n3}(u)) + \alpha_3 a_3(u)], \\ v_{14}(u) &= \widehat{k}_4^{-1}(a_4(u), \mu_{k4}(u))[-\widehat{h}_4(a_4(u), \mu_{n4}(u)) + \alpha_4 a_4(u)]. \end{aligned} \tag{95}$$

Where $\widehat{h}_l$ and $\widehat{k}_l$ are $T3-FLSs$. The parameters of FLS are considered in Table 1.

Table 1: Parameters of FLS

Parameter	**Value**
$J_{\tilde{\mu}_l^1}, J_{\tilde{\mu}_l^2}, J_{\tilde{\mu}_l^3}$	-1, 0, 1
$\overline{\Delta}_{\tilde{\mu}_l^m}$	0.5
$\underline{\Delta}_{\tilde{\mu}_l^m}$	0.5
$\overline{r}$	0.7, 0.8, 0.9
$\underline{r}$	0.2, 0.3, 0.4
p_s	9

Where the other parameters and control matrices are

$$\begin{aligned} \alpha_1 &= \begin{bmatrix} 0 & 1 \\ -\eta_{1,1} & -\eta_{1,2} \end{bmatrix} \alpha_{e1} = x_{e1} \times \begin{bmatrix} 1 & 0 \\ 0 & 1 \end{bmatrix}, \\ \alpha_2 &= \begin{bmatrix} 0 & 1 \\ -\eta_{2,1} & -\eta_{2,2} \end{bmatrix} \alpha_{e2} = x_{e2} \times \begin{bmatrix} 1 & 0 \\ 0 & 1 \end{bmatrix}, \\ \alpha_3 &= \begin{bmatrix} 0 & 1 \\ -\eta_{3,1} & -\eta_{3,2} \end{bmatrix} \alpha_{e3} = x_{e3} \times \begin{bmatrix} 1 & 0 \\ 0 & 1 \end{bmatrix}, \\ \alpha_4 &= \begin{bmatrix} 0 & 1 \\ -\eta_{4,1} & -\eta_{4,2} \end{bmatrix} \alpha_{e4} = x_{e4} \times \begin{bmatrix} 1 & 0 \\ 0 & 1 \end{bmatrix}. \end{aligned} \tag{96}$$

The parameters are set as $\eta_{l,1} = \eta_{l,2} = 0.10, l = 1, 2, 3, 4$ and $x_{e1} = 0.2, x_{e2} = 0.25, x_{e3} = 0.40, x_{e4} = 0.60$ by using weighting matrices $Y_d = diag\{0.01, 0.01\}, Y_v = 0.01$ to solve the optimization problem of Theorem (5.1) online produces $v_{2l}, l = 1, ...4$ by applying distributed controller $v_1(u) = v_{11}(u) + v_{21}(u), v_2(u) = v_{12}(u) + v_{22}(u), v_3(u) = v_{13}(u) + v_{23}, v_4(u) = v_{14}(u) + v_{24}(u)$ the consensus error dynamics of 53 are stabilized.

Moreover, time delay effects are analyzed. The RMSE values are balanced, and the delay samples are changed. The RMSEs are introduced in Table (2). The accuracy of the controller remains unaffected by the presence of various time delay samples. Further, the lower RMSE is the result of $T3-FLSs$, which is shown in Table (3). It is introduced in table (2) and table 3; Multiple time delays have no impact on the authenticity. By the suggested distributed control scheme, a part of the uncertainties is managed because of the impact of time delay. The controller managed and estimated the robot dynamics of uncertainties and perturbations at each sample time.

Table 2: Time Delay Effect.

State	1	5	10
a_{11}	1.2651	1.2670	1.3021
a_{12}	1.0137	1.0172	1.0201
a_{21}	1.3560	1.3641	1.3692
a_{22}	1.0200	1.0205	1.0212
a_{31}	1.5083	1.5302	1.6301
a_{32}	1.0290	1.0322	1.0392
a_{41}	2.4010	2.4105	2.4532
a_{42}	1.0738	1.0802	1.0890

Table 3: FLSs comparison.

State	T3-FLS	T2-FLS	T1-FLS
a_{11}	1.2651	1.8710	2.0678
a_{12}	1.0137	1.9850	2.2001
a_{21}	1.3560	1.5101	1.7041
a_{22}	1.0200	1.8501	2.0254
a_{31}	1.5083	1.5241	1.6950
a_{32}	1.0290	1.7014	2.0025
a_{41}	2.4010	2.5155	2.6036
a_{42}	1.0738	1.7408	1.9052

Below, we present MATLAB simulations.

Figures (4) and (5) show the first state response of robots under the MPC Type-3 Fuzzy controller and Show the second state response of robots under the MPC Type-3 Fuzzy controller, respectively. Figures (6) and (7) show the approximation error and consensus error between robots, respectively. Figures (8) and (9) the first control input response and second control input signal response for four robots, respectively. Figures (10) and (11) show the controller response under sensor attacks and actuator attacks for four robots, respectively. Figure (12) shows the controller performance under both sensor and actuator attacks.

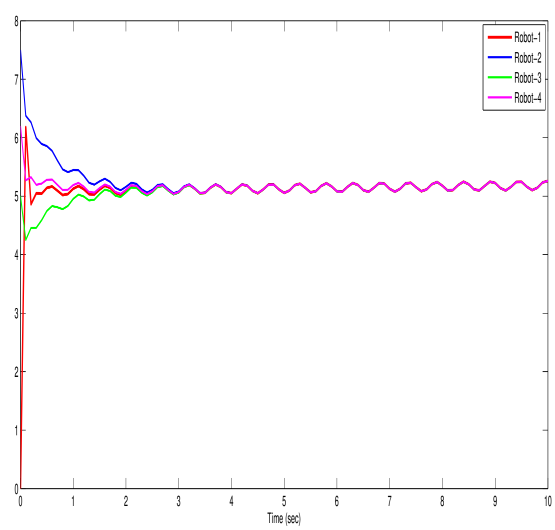

Figure 4: Shows the first state response of robots under the MPC Type-3 Fuzzy controller.

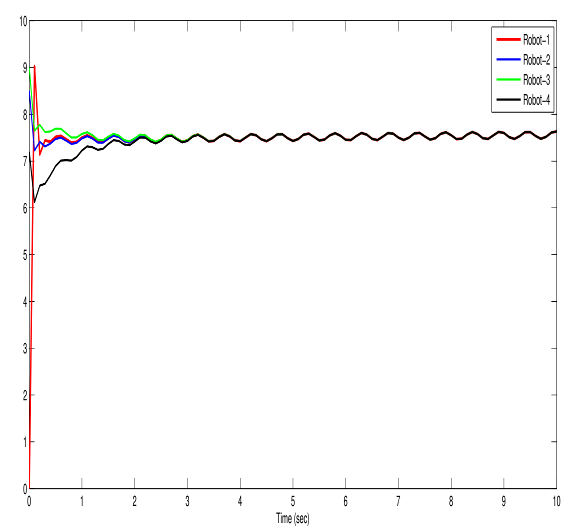

Figure 5: Shows the second state response of robots under the MPC Type-3 Fuzzy controller.

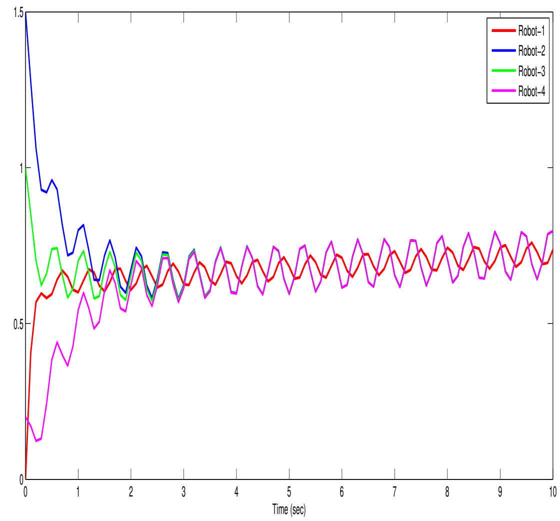

Figure 6: Shows the approximation error between the robots.

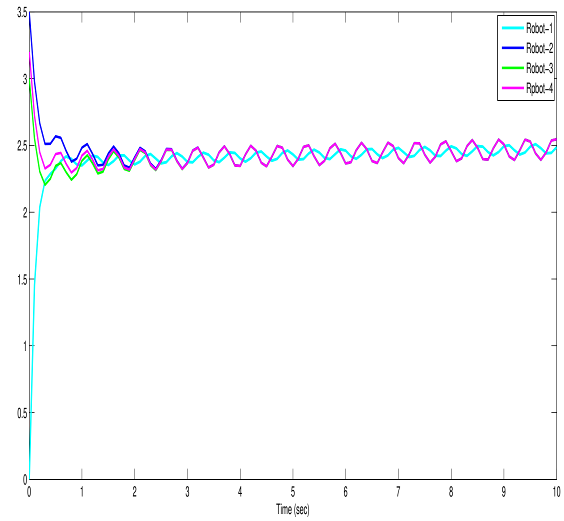

Figure 7: Shows the consensus error between the robots.

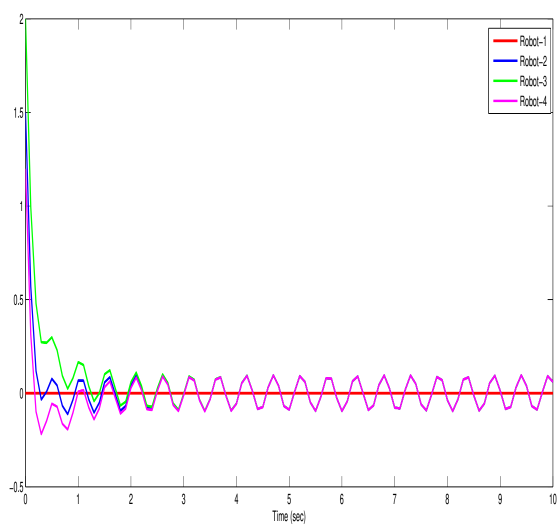

Figure 8: Shows the first control input response for four robots.

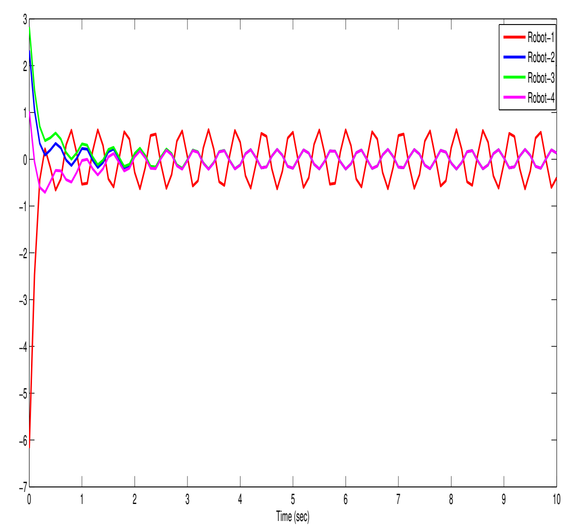

Figure 9: Shows the second control input response for four robots.

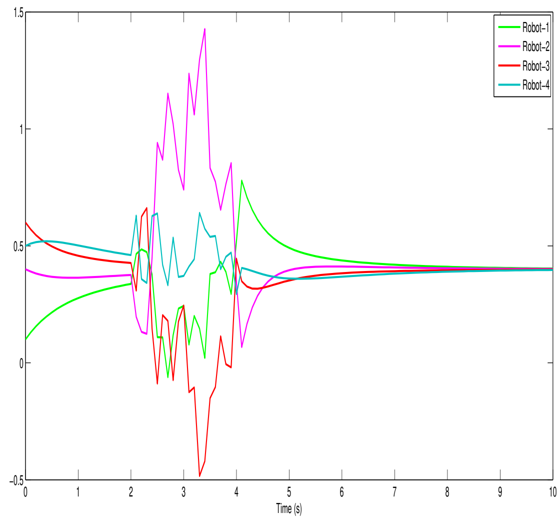

Figure 10: Shows the controller response under the sensor attack of robots.

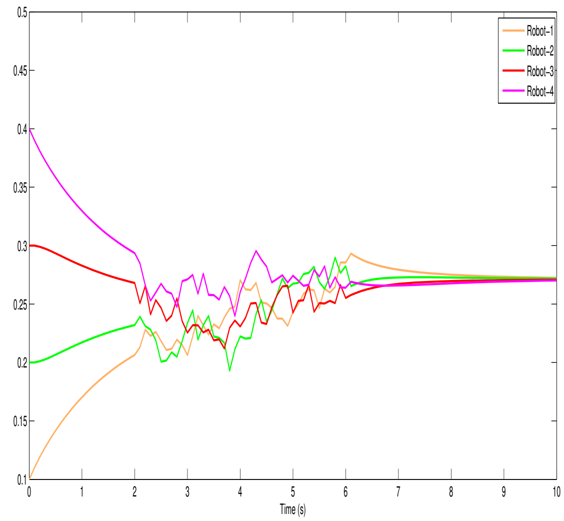

Figure 11: Shows the controller response under the actuator attack of robots.

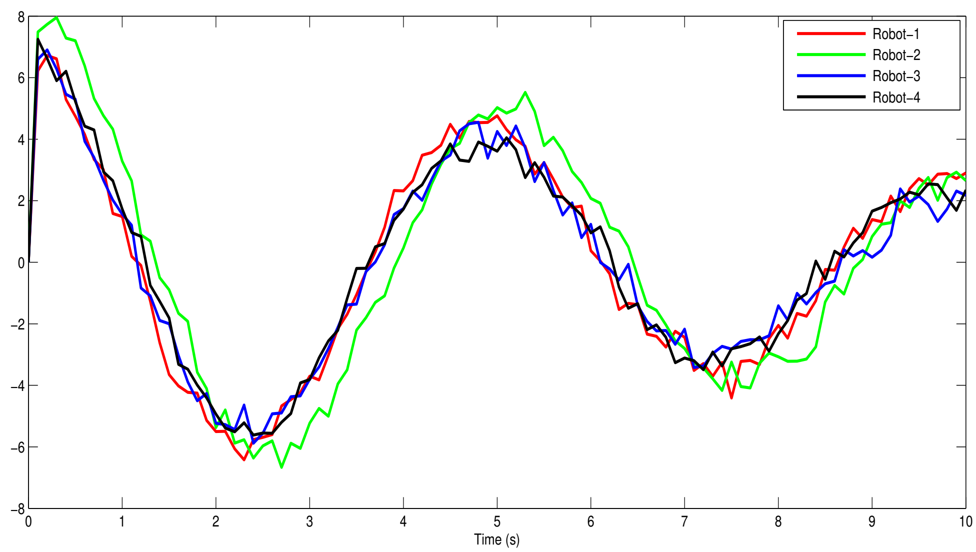

Figure 12: Shows the overall control input response under the sensor and actuator attacks.

The simulation results in Figures (13) to (20) validate the effectiveness of the proposed multi-robot control framework. Figure (13) shows the 3D state evolution, confirming that all robots converge to a coordinated motion. Figure (14) presents the consensus error surface, where errors steadily decay to zero, indicating successful consensus achievement. The control input behavior in Figure (15) remains bounded and smooth, demonstrating practical actuator feasibility. Figure (16) illustrates system performance under attack conditions, showing that stability is preserved despite disturbances. The delay robustness is verified in Figure (17), where convergence is maintained under different communication delays. Figure (18) confirms stability through the decreasing Lyapunov function for all robots. The nonlinear motion behavior is depicted in Figure (19), where all trajectories show consistent convergence in phase space. Finally, Figure (20) represents the inter-robot interaction structure, highlighting effective network coupling for consensus achievement.

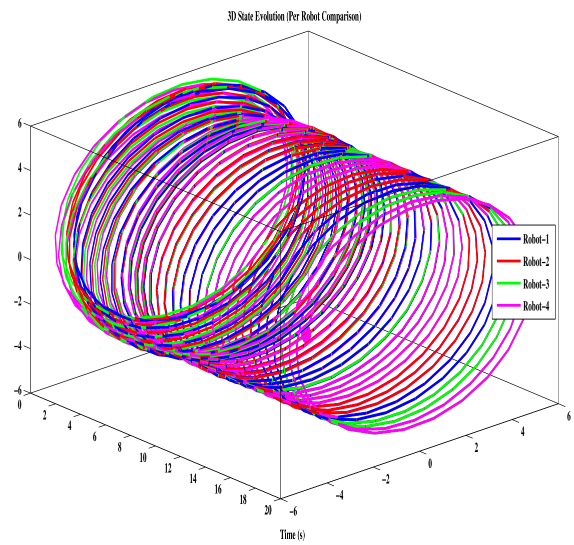

Figure 13: 3D state evolution showing robot-wise convergence behavior over time.

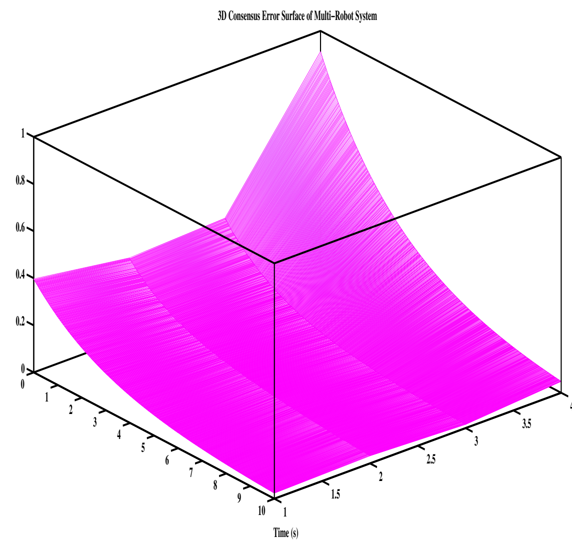

Figure 14: 3D consensus error surface illustrating decay of inter-robot disagreement.

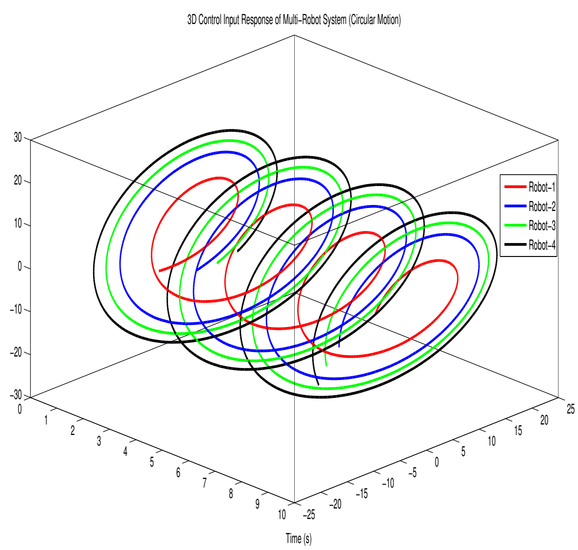

Figure 15: 3D control input response demonstrating bounded and smooth actuator effort.

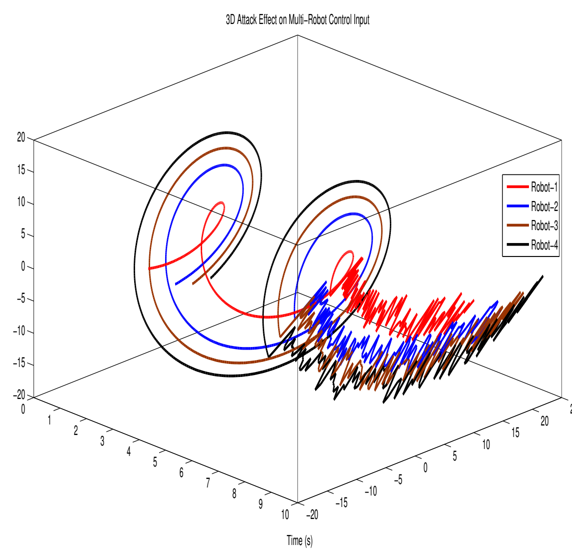

Figure 16: 3D attack impact visualization under sensor and actuator disturbances.

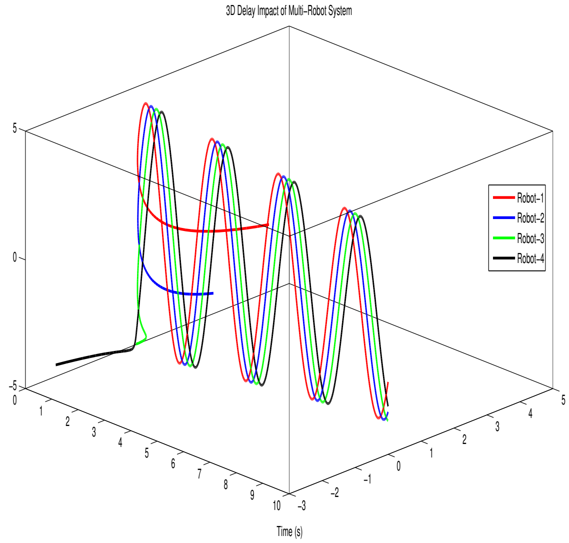

Figure 17: 3D delay impact showing robustness under communication delays.

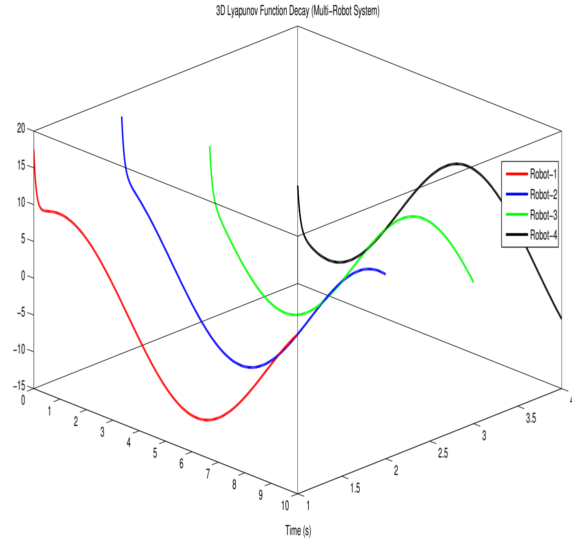

Figure 18: 3D Lyapunov function decay confirming system stability for all robots.

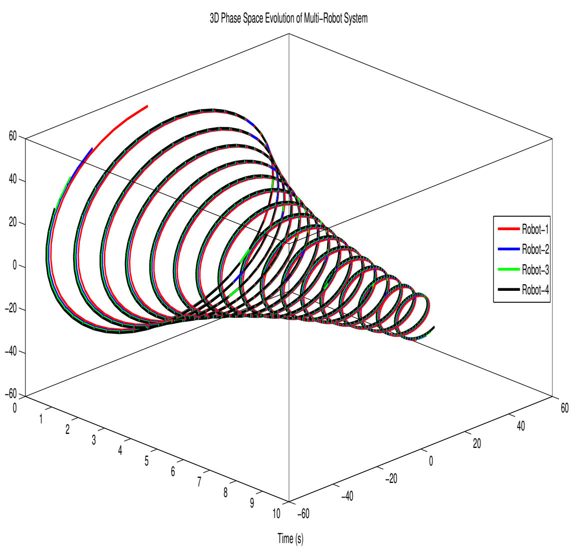

Figure 19: 3D phase space trajectories illustrating nonlinear robot motion behavior.

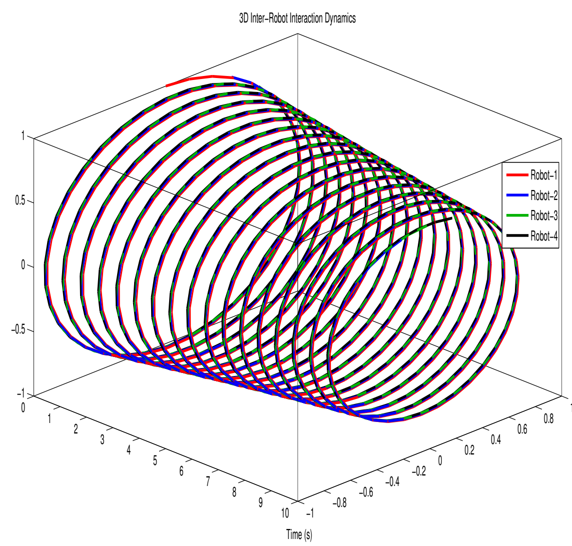

Figure 20: 3D inter-robot interaction showing network coupling strength.

For Example (6.1), the suggested algorithm is also contrasted with standard MPC, LQR, and SMC algorithms. The outcomes prove that the suggested technique offers faster convergence and increased robustness against disturbances and attacks.

7 Conclusion

The method proposed in this paper enables the multi-robot system to operate effectivelyunder time delays and cyber-physical distributed cyber-physical attacks, including sensor and actuator attacks. The combination of Type-3 Fuzzy Logic Systems (T3-FLS) and Model Predictive Control (MPC) is used to achieve this. To deal with uncertainties and the nonlinear behavior of each robot, a fuzzy logic system is used to adjust the control rules in real-time. MPC helps in the decision-making process, which also helps to manage the resource limits, such as not overloading the control signals. To reduce the impact of possible cyber attacks, security constraints are added to the controller. This way, the system can still function properly under sensor and actuator attacks. Duffing-Holmes chaotic model is used in system performance, having sensitive and complex behavior, which handles delays and attacks successfully; the robots could still stay coordinated and perform well, even under cyber-physical disruption or defined attacks. The example also shows that the robots follow the smooth path without instability in their control signals. Furthermore, a comparison with Type-1 and Type-2 fuzzy logic systems shows us that the new Type-3 fuzzy system is more effective. In future work, the study will be on how to make the Type-3 fuzzy system even more effective and how well the control method performs when actuator attacks are present in the system.

Funding

This article is supported by the National Natural Science Foundation of China (12301185), the Natural Science Research Project of Universities and Colleges in Anhui Province under Grant 2023AH052548.

Acknowledgments

This work has been carried out at the University of Lahore, Sargodha Campus and Hefei Technology College, China. The authors are also grateful for the support from the University of Mianwali and Al Ahliyya Amman University, Amman, Jordan.

Competing interests: The authors have no relevant financial or non-financial interests to disclose.

Data availability: Data sharing not applicable to this article as no datasets were generated or analysed during the current study.

Code Availability: The code is considered an intellectual property of the University of Lahore, Sargodha Campus, Pakistan, and therefore not publicly available.

Author contributions: Conceptualization, Ping Yu; Software, Naveed Iqbal; Validation, Aseel Smerat; Formal analysis, Abeeha Mishal; Resources, Ping Yu; Writing - original draft, Waqar Ul Hassan, Ping Yu; Writing-review & editing, Waqar Ul Hassan, Ping Yu; Supervision, Azmat Ullah Khan Niazi; Project administration, Ping Yu.

Use of generative-AI tools declaration: The authors declare that they have not used Artificial Intelligence (AI) tools in the creation of this article.

References

[1] B. Cai, S. Zhang, H. Zhu, X. Ju, Y. Zhao, *Manifold-constraint anti-disturbance subspace predictive control for unmodeled free-floating space robot maneuvering*, Aerospace Science and Technology, **177**(Part B) (2026), 112256. https://doi.org/10.1016/j.ast.2026.112256

[2] P. Chen, Y. Song, Y. Xia, *Adaptively diagnosing system faults in microservice architecture: An autonomous predictive model construction framework*, Future Generation Computer Systems, **177** (2026), 108256. https://doi.org/10.1016/j.future.2025.108256

[3] Q. Chen, R. Wu, D. Schott, J. Jovanova, *Programmable structure with shape memory materials for soft robotics*, Smart Materials and Structures, **35**(1) (2026), 15049. https://doi.org/10.1088/1361-665X/ae2a85

[4] J. Chen, C. Yu, Y. Wang, Z. Zhou, Z. Liu, *Hybrid modeling for vehicle lateral dynamics via AGRU with a dual-attention mechanism under limited data*, Control Engineering Practice, **151** (2024), 106015. https://doi.org/10.1016/j.conengprac.2024.106015

[5] F. Ding, Z. Liu, Y. Wang, et. al., *Intelligent event triggered lane keeping security control for autonomous vehicle under DoS attacks*, IEEE Transactions on Fuzzy Systems, **33**(10) (2025), 3595-3608. https://doi.org/10.1109/TFUZZ.2025.3597276

[6] X. Du, J. Zhu, J. Zhou, et. al., *DP-TRAE: A dual-phase merging transferable reversible adversarial example for image privacy protection*, IEEE Transactions on Dependable and Secure Computing, **22**(6) (2025), 7849-7861. https://doi.org/10.1109/TDSC.2025.3601175

[7] S. Fan, J. Chang, Z. Wang, et. al., *Research on adaptive cooperative positioning algorithm for underwater robots based on dolphin group cooperative mechanism*, Biomimetics, **11**(1) (2026), 82. https://doi.org/10.3390/biomimetics11010082

[8] B. Feng, Z. Wang, L. Yuan, Q. Zhou, Y. Chen, Y. Bi, *Towards safe motion planning for industrial human-robot interaction: A co-evolution approach based on human digital twin and mixed reality*, Robotics and Computer-Integrated Manufacturing, **95** (2025), 103012. https://doi.org/10.1016/j.rcim.2025.103012

[9] Y. Fu, B. Wang, H. Zhao, M. Zhou, N. Li, Z. Gao, *Adaptive safety attitude control of a hybrid VTOL UAV under transition flight subject to multiple faults and uncertainties*, Aerospace Science and Technology, **163** (2025), 110284. https://doi.org/10.1016/j.ast.2025.110284

[10] Y. Guan, L. Yang, Z. Li, et. al., *A novel variable-morphology soft robot inspired by inchworms and pangolins using a combination of magnetoelastic and thermoelastic materials*, Colloids and Surfaces A: Physicochemical and Engineering Aspects, **747** (2026), 140889. https://doi.org/10.1016/j.colsurfa.2026.140889

[11] W. Guo, J. Liu, W. Qin, X. Lan, H. Bai, X. Li, *Robust adaptive dynamic programming for morphing air-breathing hypersonic vehicles under unmatched uncertainty*, Science China Information Sciences, **69**(2) (2026), 122205. https://doi.org/10.1007/s11432-024-4386-4

[12] C. Guo, G. Zhong, Z. Xiao, D. Wang, *Detecting faulty substructures in networks*, IEEE Transactions on Computers, **75**(5) (2026), 1937-1948. https://doi.org/10.1109/TC.2026.3661204

[13] F. Hongguang, K. Shi, A. Zhou, F. Meng, L. Jiang, *Exploring fixed-time synchronization of fractional-order fuzzy cellular neural networks with information interactions and time-varying delays via adaptive multi-module control*, Fractal and Fractional, **10**(4) (2026), 253. https://doi.org/10.3390/fractalfract10040253

[14] M. Hou, J. Zhao, J. Tian, H. Du, *Minimum operator-based data-driven sliding mode control for a magnetorheological fluid dual clutch*, IEEE Transactions on Cybernetics, **55**(10) (2025), 4991-5001. https://doi.org/10.1109/TCYB.2025.3596063

[15] Y. Hou, S. Zhong, Z. Zheng, *Magnetic shaftless propeller millirobot with multimodal motion for small-scale fluidic manipulation*, Cyborg and Bionic Systems, **6** (2025), 0235. https://doi.org/10.34133/cbsystems.0235

[16] M. Huo, Z. Fan, J. Qi, N. Qi, D. Zhu, *Fast analysis of multi-asteroid exploration mission using multiple electric sails*, Journal of Guidance, Control, and Dynamics, **46**(5) (2023), 1015-1022. https://doi.org/10.2514/1.G006972

[17] Y. Jiang, P. Chen, Q. Guo, et. al., *A novel posture optimization method based on the comprehensive stiffness performance index in robotic milling*, Journal of the Brazilian Society of Mechanical Sciences and Engineering, **48**(6) (2026), 445. https://doi.org/10.1007/s40430-026-06446-y

[18] J. Jin, L. Zhao, L. Chen, W. Chen, *A robust zeroing neural network and its applications to dynamic complex matrix equation solving and robotic manipulator trajectory tracking*, Frontiers in Neurorobotics, **16** (2022), 1065256. https://doi.org/10.3389/fnbot.2022.1065256

[19] Y. Kang, L. Yao, H. Wang, *Fault isolation and fault-tolerant control for Takagi–Sugeno fuzzy time-varying delay stochastic distribution systems*, IEEE Transactions on Fuzzy Systems, **30**(4) (2022), 1185-1195. https://doi.org/10.1109/TFUZZ.2021.3053320

[20] R. Li, J. Jin, D. Zhang, C. Chen, *A segmented activation function-based zeroing neural network model for dynamic Sylvester equation solving and robotic manipulator control*, Concurrency and Computation: Practice and Experience, **37**(21-22) (2025), e70243. https://doi.org/10.1002/cpe.70243

[21] G. Li, X. Liang, J. Zhang, T. Su, Z. Hou, *A stiffness-enhanced extensible continuum surgical robot: Design, modeling, and evaluation*, IEEE/ASME Transactions on Mechatronics, **31**(1) (2025), 413-424. https://doi.org/10.1109/TMECH.2025.3592964

[22] D. Li, S. Ren, H. Wang, J. Liu, S. S. Ge, *Randomized average consensus based on additive privacy sharing*, Automatica, **186** (2026), 112847. https://doi.org/10.1016/j.automatica.2026.112847

[23] F. J. Li, H. Y. Zhang, Z. L. Lu, et. al., *Unsupervised learning enabled label-free single-pixel imaging for resilient information transmission through unknown dynamic scattering media*, Opto-Electronic Advances, **8**(10) (2025), 250013. https://doi.org/10.29026/oea.2025.250013

[24] W. Liang, X. Sun, Y. Ji, J. Wu, X. Liu, *Anonymous dynamic formation control of multiagent systems with obstacle avoidance*, IEEE Transactions on Reliability, **75** (2026), 1079-1093. https://doi.org/10.1109/TR.2026.3665586

[25] Q. Liu, P. Chen, K. Lin, K. Zhao, J. Ding, Y. Li, *Sample-efficient backtrack temporal difference deep reinforcement learning*, Knowledge-Based Systems, **330**(Part B) (2025), 114613. https://doi.org/10.1016/j.knosys.2025.114613

[26] R. Liu, Y. Fan, et. al., *Design and workspace analysis of a cable-driven space capture robot for noncooperative targets*, Proceedings of the Institution of Mechanical Engineers, Part G: Journal of Aerospace Engineering, **238**(14) (2024), 1406-1418. https://doi.org/10.1177/09544100241272826

[27] Q. Liu, Z. Song, Y. Liang, Z. Xie, et. al., *CoRLHF: Reinforcement learning from human feedback with cooperative policy-reward optimization for LLMs*, Expert Systems with Applications, **301** (2026), 130113. https://doi.org/10.1016/j.eswa.2025.130113

[28] X. Liu, C. Wu, S. Zhen, H. Sun, C. Sun, Y. Chen, *Robust control under servo constraint following via Nash equilibrium theory for bimanual humanoid manipulation*, IEEE Transactions on Fuzzy Systems, **33**(11) (2025), 4069-4082. https://doi.org/10.1109/TFUZZ.2025.3609828

[29] R. Liu, H. Yang, W. Li, et. al., *Intelligent form-finding and optimization of six-bar tensegrity deployable antennas for enhanced prestress distribution and surface accuracy*, Structural and Multidisciplinary Optimization, **69**(5) (2026), 131. https://doi.org/10.1007/s00158-026-04339-1

[30] Z. Lu, X. Zhang, X. Cao, J. Hou, X. Yuan, *SFEP-YOLO: A track obstacle detection model for autonomous electric locomotives in underground mine*, IEEE Transactions on Vehicular Technology, **75**(6) (2026), 9687-9700. https://doi.org/10.1109/TVT.2026.3651888

[31] Z. Luan, W. Zhao, C. Wang, *Coordinated tracking control of the integrated wheel-end system based on generalized instantaneous steering center constraint*, IEEE Transactions on Transportation Electrification, **11**(3) (2025), 8271-8281. https://doi.org/10.1109/TTE.2025.3538892

[32] G. Nongyue, X. Changchuan, A. Chao, C. Zhiying, S. Chen, *Unified aeroelastic and flight dynamics formulation based on state-space unsteady aerodynamics*, AIAA Journal, **64**(5) (2026), 1-18. https://doi.org/10.2514/1.J065498

[33] Y. Shi, Z. Li, Z. Yang, et. al., *Neural-based adaptive grinding force tracking control for pneumatic end-actuator with uncertain dynamic model constraints*, Information Sciences, **728** (2026), 122813. https://doi.org/10.1016/j.ins.2025.122813

[34] Y. Sun, H. Sun, J. Ma, et. al., *Multimodal agent AI: A survey of recent advances and future directions*, Journal of Computer Science and Technology, **40**(4) (2025), 1046-1063. https://doi.org/10.1007/s11390-025-4802-8

[35] Y. Tian, H. Tian, *A multi-layer dynamic model of information propagation considering individual three-phase linear modulated behaviors*, Physica A: Statistical Mechanics and its Applications, **689** (2026), 131427. https://doi.org/10.1016/j.physa.2026.131427

[36] Q. Wang, J. Cao, H. Liu, *Adaptive fuzzy control of nonlinear systems with predefined time and accuracy*, IEEE Transactions on Fuzzy Systems, **30**(12) (2022), 5152-5165. https://doi.org/10.1109/TFUZZ.2022.3169852

[37] G. Wang, Z. Feng, Y. Qu, H. Sun, *Event-triggered adaptive predefined-time anti-unwinding attitude tracking control for spacecraft*, PLoS One, **20**(10) (2025), e0333700. https://doi.org/10.1371/journal.pone.0333700

[38] W. Wang, J. Jiang, W. Wang, et. al., *Design and analysis of a self-orienting wireless power transfer system for the multifunctional capsule robot*, IEEE Transactions on Power Electronics, **41**(5) (2026), 8624-8635. https://doi.org/10.1109/TPEL.2025.3635774

[39] Y. Wang, Z. Zhang, X. Yuan, X. Yin, *Constraint control of electro-hydraulic position servo system based on command filter*, Transactions of the Canadian Society for Mechanical Engineering, **50** (2026), 1-12. https://doi.org/10.1139/tcsme-2025-0142

[40] M. Wang, D. Zhou, M. Chen, *Hybrid variable monitoring: An unsupervised process monitoring framework with binary and continuous variables*, Automatica, **147** (2023), 110670. https://doi.org/10.1016/j.automatica.2022.110670

[41] T. Wang, Z. Zhu, X. Zhou, T. Jing, W. Chen, *A function-based behavioral modeling method for air combat simulation*, Journal of Systems Engineering and Electronics, **35**(4) (2024), 945-954. https://doi.org/10.23919/JSEE.2024.000068

[42] W. Xiao, C. Xie, Y. Xiao, et. al., *A new vacuum-powered soft bending actuator with programmable variable curvatures*, Materials and Design, **250** (2025), 113641. https://doi.org/10.1016/j.matdes.2025.113641

[43] J. Xie, H. Liu, S. Nie, C. Xiang, L. Han, *Jumping in legged robots: A review of advances in jumping abilities, methods, challenges, and future directions*, Robotics and Autonomous Systems, **201** (2026), 105434. https://doi.org/10.1016/j.robot.2026.105434

[44] J. Xiong, X. Wang, *Adaptive sliding mode control for uncertain tilting quadrotors using randomized feedforward neural networks*, International Journal of Robust and Nonlinear Control, **36**(7) (2026), 4042-4055. https://doi.org/10.1002/rnc.70396

[45] F. Xu, S. Feng, Y. Wang, J. Chang, C. Zhou, *Efficient deep reinforcement learning with expert demonstrations for human-machine shared steering control under emergency obstacle avoidance conditions*, IEEE Transactions on Vehicular Technology, **75**(5) (2026), 7356-7367. https://doi.org/10.1109/TVT.2025.3629701

[46] Z. Xu, K. Wang, C. Mu, T. Qiu, *Safety-critical path planning for obstacle avoidance based on reinforcement learning and control barrier functions*, IEEE Internet of Things Journal, **12**(23) (2025), 51410-51421. https://doi.org/10.1109/JIOT.2025.3614857

[47] Z. Yan, Z. Pan, G. Hu, J. Cheng, W. Qi, *Annular finite-time H_2/H_∞ control for mean-field jump-diffusion systems*, IEEE Transactions on Cybernetics, **55**(11) (2025), 5358-5371. https://doi.org/10.1109/TCYB.2025.3597588

[48] Z. Yang, J. Shu, J. Jiang, et. al., *Automated path-planning strategy for robotic inspection of underground utilities based on building information model*, Computer-Aided Civil and Infrastructure Engineering, **40**(29) (2025), 5554-5575. https://doi.org/10.1111/mice.70107

[49] X. Yang, X. Zhang, J. Cao, H. Liu, *Observer-based adaptive fuzzy fractional backstepping consensus control of uncertain multiagent systems via event-triggered scheme*, IEEE Transactions on Fuzzy Systems, **32**(7) (2024), 3953-3967. https://doi.org/10.1109/TFUZZ.2024.3386312

[50] Z. Yang, W. Zhao, J. Kou, et. al., *Observer-based fuzzy adaptive dynamic surface force control for pneumatic polishing system end-effector with uncertain contact environment model*, IEEE Transactions on Automation Science and Engineering, **22** (2025), 17898-17913. https://doi.org/10.1109/TASE.2025.3585136

[51] C. Ye, Y. Yao, W. Lin, X. Yang, J. Qiu, *CSGrasp: Category-level semantically-aware grasping method*, IEEE Transactions on Industrial Electronics, **73**(2) (2026), 2610-2619. https://doi.org/10.1109/TIE.2025.3605439

[52] W. Yuan, J. Chen, S. Chen, D. Feng, et. al., *Transformer in reinforcement learning for decision-making: A survey*, Frontiers of Information Technology and Electronic Engineering, **25**(6) (2024), 763-790. https://doi.org/10.1631/FITEE.2300548

[53] Z. Zhang, R. He, B. Han, S. Ren, J. Fan, H. Wang, Z. Ma, *Magnetically switchable adhesive millirobots for universal manipulation in both air and water*, Advanced Materials, **37**(26) (2025), 2420045. https://doi.org/10.1002/adma.202420045

[54] Y. Zhang, Y. Shen, Y. C. Soh, et. al., *Directionally regularized two-stage calibration for cross-shaped MGT sensor arrays with physics-inspired error modeling*, IEEE Transactions on Instrumentation and Measurement, **75** (2026), 1-12. https://doi.org/10.1109/TIM.2026.3660392

[55] Y. Zhang, Y. Wang, C. Su, et. al., *Multi-sensor fusion-based intelligent auxiliary system of power wheelchairs for individuals with limbs disabilities: Design and implementation*, Measurement, **257**(Part A) (2026), 118573. https://doi.org/10.1016/j.measurement.2025.118573

[56] S. Zhen, W. Ye, X. Liu, *A leakage-type adaptive robust control method for collaborative robot joints with fuzzy uncertainty: Trajectory constraints and parameter optimization*, Information Sciences, **754** (2026), 123674. https://doi.org/10.1016/j.ins.2026.123674

[57] H. Zhong, H. Zhang, S. Zhen, et. al., *Adaptive robust control for underactuated bipedal parallel wheel-legged robots: A Nash game-based constraint following approach*, IEEE Transactions on Fuzzy Systems, **34**(6) (2026), 1791-1803. https://doi.org/10.1109/TFUZZ.2026.3670620

[58] M. Zhong, J. Zhang, G. Zheng, H. Liu, *Data–driven model–free adaptive dynamic programming resilient control for nonlinear networked control systems under DoS attacks*, IEEE Transactions on Cybernetics, **55**(12) (2025), 5700-5713. ://doi.org/10.1109/TCYB.2025.3594793

[59] L. Zhou, Z. Li, Y. Li, S. Bai, *Parallel MPPI with gradient-velocity modulated SDF cost for high-performance real-time dynamic obstacle avoidance by robot manipulators*, IEEE Transactions on Robotics, **41** (2025), 5149-5168. https://doi.org/10.1109/TRO.2025.3600125

[60] X. Zhou, L. Li, X. Zhang, S. Jin, et. al., *A seventy-year review of Dubins robot path planning: Basics, developments and opportunities*, Industrial Robot: The International Journal of Robotics Research and Application, (2026), 1-23. https://doi.org/10.1108/IR-07-2025-0265